Effect of Pretwist on Aeroelastic Response of a Rotor System with Dynamic Stall and Dynamic Wake

V. Laxman[1] and C. Venkatesan[2]

Department of Aerospace Engineering,

Indian Institute of Technology Kanpur, India.

Abstract

Flight test data of helicopters indicate that vibratory levels in the fuselage exhibit a wide spectrum of frequencies including the dominant blade passage frequency and its integer multiples. The present work attempts to understand the reason for the existence of several frequencies in the response of the fuselage and possible cause for this observed phenomenon by formulating a computational aeroelastic model. In this study, the effect of pretwist on the trim condition and aeroelastic response of a rotor system with dynamic stall and dynamic wake has been analysed. The differential equations of motion are solved in time domain in a sequential manner to obtain the response of all the blades in the rotor system, the inflow variables, and the sectional loads at every time step. The influence of aerodynamic modeling on the trim condition of the rotor blade in forward flight has been brought out. It is found that the aerodynamic model incorporating dynamic wake and dynamic stall effects predict the trim parameters whose variation with forward speed resemble qualitatively similar to those obtained in flight test. It is shown that the structural coupling due to blade pretwist significantly influences the rotor blade response and loads compared to an untwisted rotor blade.

1 Nomenclature

a_d, a_l, a_m	parameters used in dynamic stall model
b	blade semi-chord

[1]Graduate Student

[2]Pandit Ramachandra Dwivedi Chair Professor (email: cven@iitk.ac.in)

C_D	unsteady drag coefficient
C_{d_L}	linear static drag coefficient extrapolated to the stall region
C_M	unsteady moment coefficient
C_{m_L}	linear static moment coefficient extrapolated to the stall region
C_t	chord of the tail rotor
C_T	main rotor thrust coefficient
C_{T_t}	tail rotor thrust coefficient
C_Z	unsteady lift coefficient
C_{z_L}	linear static lift coefficient extrapolated to the stall region
C_{D_0}	zero-lift drag coefficient
$[\overline{C}]$	damping matrix in modal space
d, d_m	parameters used in dynamic stall model
D	drag on airfoil or fuselage drag
f	fuselage frontal area
$\{\overline{F}\}$	generalized aerodynamic load vector
H	longitudinal force
k_x, k_y	inflow parameters in Drees model
K_n^m	parameter used in dynamic wake model, $\frac{2}{\pi}\ H_n^m$
$[\overline{K}]$	stiffness matrix in modal space
L	lift on airfoil
$[L]$	coupling or gain matrix
$[\tilde{\mathbf{L}}^{\mathbf{c}}]$, $[\tilde{\mathbf{L}}^{\mathbf{s}}]$	cosine and sine influence coefficient matrices
M	moment on airfoil about elastic axis or Mach number
M_x, M_y, M_z	rolling, pitching and yawing moment
$[M]$	mass matrix or apparent mass matrix in inflow model
$[\overline{M}]$	mass matrix in modal space
n, j	polynomial number

N_b	number of blades
$P_j^p(\overline{\nu})$	Legendre polynomial functions
$\bar{P}_j^p(\overline{\nu})$	normalised Legendre polynomial functions, $(-1)^p \ P_j^p \ (\overline{\nu})/\rho_j^p$
r	radial distance
$\overline{r}$	nondimensional radial coordinate, $\frac{r}{R}$
r_d, r_l, r_m	parameters used in dynamic stall model
R	rotor blade radius
R_t	radius of the tail rotor
$\tilde{S}$	area of airfoil
s_h	horizontal tail area
s_v	vertical tail area
S_ϕ	static moment about elastic axis
t	time
T	main rotor thrust force
T_t	tail rotor thrust force
V	oncoming velocity
V_F	velocity at helicopter centre of mass
V_H	velocity of the hub
V_T, V_R	velocity terms used in inflow models
$[V]$, $[V_c]$, $[V_s]$	velocity matrices used in dynamic inflow models
W	weight of the helicopter
X, l	parameters defined in dynamic wake model
Y	lateral force
α	rotor shaft tilt angle *w.r.t.* helicopter forward velocity
$\tilde{\alpha}$, $\tilde{k}$	parameters used in dynamic stall model
α_j^p, β_j^p	induced flow coefficients
χ	wake skew angle

Δt	time step
ϕ_j^p	radial shape functions
Φ	fuselage attitude in roll
Γ_1	aerodynamic state in unstalled region in lift equation
Γ_2	aerodynamic state in stalled region in lift equation
Γ_{d_2}	aerodynamic state in stalled region in drag equation
Γ_{m_2}	aerodynamic state in stalled region in moment equation
λ	total inflow ratio
λ_i	induced inflow ratio
λ_u, λ_0	uniform inflow ratio
λ_t	tail rotor inflow
$\{\eta\}$	vector of modal degrees of freedom
μ	advance ratio
θ	pitch angle in degree
θ_{FP}	flight path angle
θ_0	mean value of pitch angle or main rotor collective pitch angle
θ_{0T}	tail rotor collective pitch angle
θ_{1c}, θ_{1s}	cyclic pitch angles
$\tilde{\theta}$	amplitude of time varying pitch angle
Θ	fuselage attitude pitch
ρ	density of air
ρ_j^p	normalised factor used in dynamic wake model, $\sqrt{\frac{(j+p)!!}{(2\ j+1)!!(j-p)!!}}$
σ, σ_d, σ_m, $\overline{\sigma_m}$	parameters used in dynamic stall model
σ_t	tail rotor solidity ratio
τ_n^{mc}, τ_n^{ms}	coefficients of pressure expansion
Ω	rotational speed (frequency) of the rotor
Ω_t	tail rotor rotating speed

ψ	azimuthal angle or nondimensional time, Ωt
ψ_k	azimuthal angle of the k^{th} blade
$(\ )_{1k}$	quantities in rotating $1k$ coordinate system
$(\ )_{3k}$	quantities in rotating $3k$ coordinate system
$(\dot{})$	derivative $w.r.t.$ time

2 Introduction

The field of rotary-wing aeroelasticity has progressed considerably in the past four decades (Refs. [1]-[3]). However because of the complexities, still there are several unresolved issues related to blade loads, blade response and vibrations (Refs. [4]-[6]). In Ref. [4], it is reported that divergent vertical oscillations are observed on most helicopter configurations and the frequencies of these oscillations are found to be in the range $3 \sim 4$ Hz which is close to the rotor rpm. Bousman in Ref. [5] has observed that at high forward speed the vibration in the helicopter is significantly influenced by frequencies other than blade passage frequency and its integer multiples (bN_b/rev, b = 1,2,3,..., where N_b is the number of blades in the rotor system). In a recent study reported in Ref. [6], the authors have shown that there is a good correlation between rotor noise and vibration measured at the floor of the cockpit. The vibratory signals are observed to have a wide spectrum of frequency contents including those below N_b/rev. There is no published open literature available on theoretical studies addressing the issue of frequencies below N_b/rev on the rotor vibratory loads. One of the possible reasons for the presence of frequencies below N_b/rev in the vibratory signal can be due to asymmetric structural/mass properties of the rotor blade system [7]. However, even when the rotor blades are identical, it is possible that asymmetry in the aerodynamic environment (due to unsteady nonlinear effects) of the rotor blades as it goes around the azimuth can lead to a vibratory signal which can have frequencies below N_b/rev. The

nonlinearities in the rotor blade aeroelasticity can arise due to: (a) moderate deformation of coupled flap-lag-torsion-axial modes (structural nonlinearity) and (b) unsteady aerodynamics including dynamic stall and wake effects (aerodynamic nonlinearity).

Structural dynamic modeling of the rotor blade representing all the geometric complexities of the rotor system and the coupled flap-lag-axial-torsion motions of the blade has reached a high level of sophistication (Refs. [8] - [10]). While formulating the aerodynamic operator, one should consider (a) unsteady aerodynamics of a rotor blade undergoing coupled pitching-plunging motion in a time varying oncoming flow, (b) induced flow (or inflow) at the rotor disc due to rotor blade wake, and (c) dynamic stall.

In the absence of a suitable three-dimensional (3-D) aerodynamic model, only two-dimensional (2-D) models are used in the aeroelastic analysis of rotor blades. The classical two-dimensional unsteady aerodynamic models for unstalled flow (attached flow) condition are: (1) Theodorsen's model [11] applicable for a pitching and plunging airfoil with zero mean angle of attack; (2) Greenberg's theory [12] for a pitching and plunging airfoil having non-zero mean angle of attack in a time varying on-coming flow; and (3) Loewy's model [13] applicable for a pitching and plunging airfoil including cascade effects (rotor wake is treated in an approximate manner for a hovering condition). Because of the simplicity for application, most of the aeroelastic studies use Greenberg's theory, taking into consideration the wake induced inflow effects (Refs. [14]-[17]).

The wake induced inflow at the rotor disc can be obtained by either prescribed wake or free wake model. These models are computationally expensive. On the other hand, dynamic inflow models are global models, which represent the unsteady wake effects of the rotor system in a simple form. In these models, the unsteady wake-induced flow through the rotor disc is defined by a set of inflow variables and these variables essentially provide a correction to the mean inflow (Ref. [18]). Extending the dynamic inflow model, Peters *et al.* (Ref. [19]) have developed a generalised wake model. In this model, the inflow distribution is represented by a set of harmonic functions and Legendre polynomials (radial shape functions).

The most complicated phenomenon of unsteady aerodynamics is dynamic stall. It is difficult to predict stall and its effect using theoretical unsteady aerodynamic tools. Hence, most of the researchers depend on empirical or semi-empirical models. Several mathematical models that attempt to predict the effects of dynamic stall are available in the literature (Refs. [20]-[25]). ONERA dynamic stall model (Ref. [23]) is a relatively simple and efficient model, which can be easily incorporated in any aeroelastic analysis. Recently, CFD methods are applied to predict aerodynamic loads on rotors and airfoils (Refs. [26] and [27]).

3 Objectives of the Present Study

In this paper, a theoretical formulation including the geometrical nonlinearities associated with structural modeling and the aerodynamic nonlinearities associated with dynamic stall has been developed. The complexity of the unsteady aerodynamic model is categorised into two cases; namely (i) evaluation of rotor inflow, and (ii) evaluation of sectional aerodynamic loads (It may be noted that this study does not address issues related to blade vortex interaction, rotor/fuselage aerodynamic interaction and radial flow effects). Different levels of models are available in the literature for inflow calculations. They are: (i) uniform inflow model based on momentum theory, (ii) Drees model, and (iii) dynamic wake model. The sectional aerodynamic loads can be evaluated by: (i) quasi-steady approximation of Greenberg's theory applicable for only attached flow conditions, and (ii) dynamic stall model applicable for both attached and separated flow. In the present study, five different combinations of aerodynamic models have been proposed and the influence of each one of these models on the trim and response characteristics of helicopter rotor in forward flight is analysed systematically.

The objectives of the present study are:

- Development of a structural dynamic model for a flexible rotor blade with and without pretwist.

- Formulation of a time domain computational aeroelastic model by integrating the structural model, the inflow model, and the dynamic stall model for the prediction of trim and response of a helicopter rotor system in forward flight.
- Formulation of a suitable computational technique for the evaluation of trim and response of a multi-bladed helicopter rotor system in forward flight. Perform a systematic analysis to identify the effects of aerodynamic modeling on the trim in forward flight.
- Study the effects of structural couplings due to blade pretwist on trim, blade response and rotor loads of a helicopter.

4 Formulation

Helicopter trim and response calculation requires all the loads acting on the helicopter system. The loads are due to (i) main rotor system (acting at the rotor hub), (ii) fuselage aerodynamic load, (iii) tail rotor hub loads, (iv) horizontal tail and vertical tail loads and (v) gravity effects. For the sake of clarity, a brief description of the loads acting on various aerodynamic surfaces is given below.

5 Main Rotor

Evaluation of aerodynamic loads require the motion of the blade at every instant. The blade response is evaluated in modal space in rotating system. The equations of motion in modal space can be written as:

$$\left[\bar{M}\right]\{\ddot{\eta}\} + \left[\bar{C}\right]\{\dot{\eta}\} + \left[\bar{K}\right]\{\eta\} = \{\bar{F}\} \tag{1}$$

where $\{\bar{F}\}$ represents the generalized aerodynamic load acting on the blade.

5.1 Inflow Model

The aerodynamic model requires evaluation of rotor inflow as a function of azimuth and radial distance. In this paper, three types of global inflow models, namely, steady uniform inflow model, Drees model and dynamic wake model, are considered. A brief mathematical description of these models is provided in the following.

(i) Uniform Inflow Model

In this model, the total inflow through the rotor disc is assumed a constant and is given as:

$$\lambda_u = \mu \tan\alpha + \lambda_i \tag{2}$$

where

$$\lambda_i = \frac{C_T}{2\sqrt{(\mu^2 + \lambda_u^2)}}$$

(ii) Drees Model

In Drees model, the rotor inflow is a function of both azimuth and radial station. It is given as:

$$\lambda(\bar{r}, \psi) = \mu \tan\alpha + \lambda_i(1 + k_x \bar{r} \sin\psi + k_y \bar{r} \cos\psi) \tag{3}$$

where

$$\lambda_i = \frac{C_T}{2\sqrt{(\mu^2 + \lambda_u^2)}}$$

$$k_x = 2\mu$$

$$k_y = \frac{4}{3}[(1 - 1.8\mu^2)\csc\chi - \cot\chi]$$

where χ is wake skew angle and it is defined as $\chi = \tan^{-1}(\mu/\lambda_u)$.

(iii) Dynamic Wake Model (Peters-He Model, Ref. [28])

In this model, the total inflow is a function of azimuth, time and radial station. It is given as:

$$\lambda(\bar{r},t,\psi) = \mu\tan\alpha + \sum_{p=0}^{\infty}\sum_{j=p+1,p+3,\ldots}^{\infty}\phi_j^p(\bar{r})[\alpha_j^p(t)\sin(p\psi) + \beta_j^p(t)\cos(p\psi)] \tag{4}$$

where α_j^p and $\beta_j^p(t)$ are evaluated by solving a set of differential equations.

$$[M]\{\dot{\alpha_j^p}\} + [V][\tilde{L}^c]^{-1}\{\alpha_j^p\} = \frac{1}{2}\{\tau_n^{mc}\} \tag{5}$$

and

$$[M]\{\dot{\beta_j^p}\} + [V][\tilde{L}^s]^{-1}\{\beta_j^p\} = \frac{1}{2}\{\tau_n^{ms}\} \tag{6}$$

In this paper, a three term approximation ($\alpha_1^0,\ \alpha_2^1$ and β_2^1) has been considered.

5.2 Sectional Aerodynamic Loads

The sectional aerodynamic loads are evaluated by using either (i) quasi-steady approximation of Greenberg's theory or (ii) *modified* ONERA dynamic stall model applicable for both attached and separated flow. For the sake of clarity, a brief mathematical description of these models is provided.

(i) Quasisteady Greenberg's Model

The quasi-steady approximation of Greenberg's theory provides time variation of lift and moment on an oscillating airfoil. The lift, moment and drag are assumed to be acting at the quarter chord point and the expressions are given below.

Lift acting normal to the resultant flow:

$$L = \frac{1}{2}\rho\tilde{S}b[\pi\dot{W}_0 + \frac{\pi}{2}\dot{W}_1] + \frac{1}{2}\rho\tilde{S}V[2\pi W_0 + 2\pi W_1] \tag{7}$$

Unsteady moment on the airfoil is given as:

$$M = \frac{1}{2}\rho\tilde{S}2b[-\frac{\pi}{4}b\dot{W}_0 - \frac{\pi}{4}VW_1 - \frac{3\pi}{16}b\dot{W}_1] \tag{8}$$

Drag acting along the resultant velocity:

$$D = \frac{1}{2}\rho\tilde{S}V^2C_{D_0} \tag{9}$$

where W_0 and W_1 are defined as $W_0 = V(\theta + \dot{h}/V)$ and $W_1 = b\dot{\theta}$. The quantities $\dot{h},\ \theta$ and V represent the heaving velocity at the elastic axis, the pitch angle and the oncoming velocity respectively.

(ii) *Modified* ONERA Dynamic Stall Model (Ref. [29])

The *modified* dynamic stall model provides time variation of lift, moment and drag on an oscillating airfoil. The stall model assumes that the lift, moment and drag are acting at the quarter chord point. The unsteady lift acting normal to the resultant velocity is given as:

$$L = \frac{1}{2}\rho\tilde{S}[sb\dot{W}_0 + kb\dot{W}_1 + V\Gamma_1 + V\Gamma_2] \tag{10}$$

where Γ_1, Γ_2 are evaluated using the following equations

$$\begin{aligned}
\ddot{\Gamma}_1 + B_2(\frac{V}{b})\dot{\Gamma}_1 + B_3(\frac{V}{b})^2\Gamma_1 &= A_3(\frac{V}{b})^2\frac{\partial Cz_L}{\partial\theta}W_0 + A_3\sigma(\frac{V}{b})^2W_1 \\
&\quad + A_2(\frac{V}{b})\frac{\partial Cz_L}{\partial\theta}\dot{W}_0 + A_2(\frac{V}{b})\sigma\dot{W}_1 \\
&\quad + A_1\frac{\partial Cz_L}{\partial\theta}\ddot{W}_0 + A_1\sigma\ddot{W}_1 \\
\ddot{\Gamma}_2 + a_l(\frac{V}{b})\dot{\Gamma}_2 + r_l(\frac{V}{b})^2\Gamma_2 &= -[r_l(\frac{V}{b})^2V\Delta Cz|_{W_0/V} + E_l(\frac{V}{b})\dot{W}_0]
\end{aligned}$$

The unsteady moment on the airfoil is given as:

$$M = \frac{1}{2}\rho\tilde{S}2b[V^2 C_{m_L}|_{W_0/V} + (\bar{\sigma}_m + d_m)b\dot{W}_0 + \sigma_m V W_1 + s_m b\dot{W}_1 + V\Gamma_{m2}] \quad (11)$$

where Γ_{m2} is evaluated using the following equation.

$$\ddot{\Gamma}_{m2} + a_m(\frac{V}{b})\dot{\Gamma}_{m2} + r_m(\frac{V}{b})^2\Gamma_{m2} = -[r_m(\frac{V}{b})^2 V\Delta Cm|_{W_0/V} + E_m(\frac{V}{b})\dot{W}_0]$$

The unsteady drag acting along the resultant velocity is given as:

$$D = \frac{1}{2}\rho\tilde{S}[V^2 C_{d_L}|_{W_0/V} + \sigma_d b\dot{W}_0 + V\Gamma_{d2}] \quad (12)$$

where Γ_{d2} is evaluated using the following equation

$$\ddot{\Gamma}_{d2} + a_d(\frac{V}{b})\dot{\Gamma}_{d2} + r_d(\frac{V}{b})^2\Gamma_{d2} = -[r_d(\frac{V}{b})^2 V\Delta Cd|_{W_0/V} + E_d(\frac{V}{b})\dot{W}_0]$$

where $\Delta Cz|_{W_0/V}, \Delta Cm|_{W_0/V}$, and $\Delta Cd|_{W_0/V}$ are the difference between the linear static aerodynamic coefficient extrapolated to the stalled region to actual static aerodynamic coefficient of lift, moment and drag respectively, measured at an effective angle of attack W_0/V. The quantities, $C_{m_L}|_{W_0/V}$ and $C_{d_L}|_{W_0/V}$ are the static moment and drag coefficients in linear regime measured at an effective angle of attack, W_0/V.

Five different combinations of aerodynamic models have been proposed and the influence of each one of these models on the trim and response characteristics of helicopter rotor in forward flight is analysed systematically. The five aerodynamic models are:

- quasi-steady aerodynamic theory (Eqs. 7 - 9) combined with uniform inflow model (Eq. 2) (QSUI),
- quasi-steady aerodynamic theory (Eqs. 7 - 9) combined with Drees model (Eq. 3) (QSDR),

- quasi-steady aerodynamic theory (Eqs. 7 - 9) combined with dynamic wake model (Eq. 4) (QSDW),
- *modified* ONERA stall model (Eqs. 10 - 12) combined with Drees model (Eq. 3) (DSDR); and
- *modified* ONERA stall model (Eqs. 10 - 12) combined with dynamic wake model (Eq. 4) (DSDW).

It may be noted that while describing the results only the abbreviations of the aerodynamic models are used for convenience.

Sectional aerodynamic loads are evaluated using either Eqs. 7 - 9 or 10 - 12. By summing up all the inertia and aerodynamic loads and integrating over the length of the blade, one can obtain the root loads. The root loads of all four rotor blades are added to obtain hubloads (H, Y, T, M_x, M_y and M_z). Mean values of the hub loads are represented by $H_0, Y_0, T_0, M_{x0}, M_{y0}$ and M_{z0}.

5.3 Tail Rotor

The thrust generated by the tail rotor is derived using combined blade element and momentum theory. The tail rotor thrust acts normal to the tail rotor plane and in a direction providing compensation to the torque of the main rotor.

Tail rotor thrust is given by (Ref. [31]):

$$T_T = C_{T_t}[\rho\pi R_t^2(\Omega_t R_t)^2] \tag{13}$$

where the coefficient of tail rotor thrust C_{T_t} is defined as:

$$C_{T_t} = \frac{\sigma_t a}{2}[\frac{\theta_{0T}}{3}(1+\frac{3}{2}\mu^2) - \frac{\lambda_t}{2}]$$

and tail rotor inflow is given by

$$\lambda_t = \frac{C_{T_t}}{2\sqrt{\mu^2 + \lambda_t^2}}.$$

5.4 Horizontal Tail

The horizontal tail is assumed to provide only aerodynamic lift. Lift is assumed as a point load acting at the quarter chord of the horizontal tail. The lift on horizontal tail is given as:

$$T_{HT} = \frac{1}{2}\rho s_h V_{HT}^2 C_{l\theta_{ht}} \theta_{ht} \tag{14}$$

where s_h is surface area and V_{HT} is oncoming velocity, which is defined as:

$$V_{HT} = \begin{cases} \mu\Omega R & \mu < 0.05 \\ \sqrt{\mu^2 + (1.8\lambda)^2}\ \ \Omega R & \mu \geq 0.05 \text{ main rotor downwash effect is added} \end{cases}$$

θ_{ht} is angle of attack and it is taken as -2 deg.

5.5 Vertical Tail

Vertical tail is assumed to provide a side force due to its lift. The load on vertical tail is obtained by using the static lift equation which is given below.

$$T_{VT} = \frac{1}{2}\rho s_v V_{VT}^2 C_{l\theta_{vt}} \theta_{vt} \tag{15}$$

where s_v is surface area and θ_{vt} is angle of attack and it is taken as 1.5 deg. The term V_{VT} it is the oncoming velocity and is defined as:

$$V_{VT} = \mu\Omega R$$

5.6 Fuselage Drag

Fuselage drag force is proportional to the square of the velocity and the frontal area. Fuselage drag can be evaluated by using following expression.

$$D = \frac{1}{2}\rho V_F^2 f C_d \tag{16}$$

where f is the equivalent frontal cross sectional area of the helicopter fuselage, C_d is drag coefficient taken as 1.0 and V_F is the oncoming velocity given as:

$$V_F = \mu\Omega R$$

Figure 1 shows the loads and orientation of the helicopter in flight. Transfering all the forces and moments due to main rotor, tail rotor, horizontal tail, vertical tail and fuselage drag to centre of gravity (CG) of the helicopter and equating to the components of the gravitational load, the equilibrium equations are obtained. In this paper, only steady level flight conditions are considered; and hence inertia effects due to maneuver are not included. The force and moment equilibrium equations are given as:

$$\begin{aligned}
H_0 + D\cos\alpha &= W\sin\Theta\cos\Phi \\
Y_0 + T_T + T_{VT} &= W\sin\Phi \\
T_0 + T_{HT} - D\sin\alpha &= W\cos\Theta\cos\Phi \\
M_{x0} - Y_0 z_{MR} + T_0 y_{MR} - (T_T z_{TR} + T_{VT} z_{VT}) + T_{HT} y_{MR} &= 0.0 \\
M_{y0} - T_0 x_{MR} + H_0 z_{MR} - T_{HT} x_{HT} &= 0.0 \\
M_{z0} + Y_0 x_{MR} - H_0 y_{MR} + (T_T x_{TR} + T_{VT} x_{VT}) &= 0.0
\end{aligned} \tag{17}$$

where $\Theta = \alpha - \theta_{FP}$. Trim variables ($\theta_0, \theta_{1c}, \theta_{1s}, \theta_{0T}, \Theta$ and Φ) can be obtained by solving the above nonlinear algebraic equations (Eq. 17).

6 Solution Procedure

The solution technique aims to obtain helicopter trim and blade response simultaneously by solving the three sets of equations in time domain, namely, (i) equations representing the elastic deformations of the rotor blade (Eq. 1), (ii) equations representing the inflow through the rotor disc (Eq. 2 or 3 or 4) and (iii) sectional aerodynamic loads representing lift, drag and moment acting on the rotor blade (Eqs. 7 - 9 or Eqs. 10 - 12). For the aerodynamic models QSUI, QSDR and QSDW, the sectional aerodynamic loads are represented by algebraic expressions given in Eqs. 7 - 9. Whereas, for the aerodynamic models DSDR and DSDW, the sectional aerodynamic loads have to be obtained by solving a set of differential equations in time domain given in Eqs. 10 - 12. Similarly for the aerodynamic models involving time varying inflow, *i.e.*, QSDW and DSDW, the inflow variables (α_1^0, α_2^1 and β_2^1) have to be obtained by solving the set of differential equations given in Eqs. 5 and 6. Of the five models used in this study, DSDW model is computationally more intensive than the other models. In this model, the time varying inflow, sectional aerodynamic loads and the blade response have to be solved by three sets of coupled ordinary differential equations, at every time step. A description on the number of variables for DSDW aerodynamic model is given in the following.

The aerodynamic loads acting on the blade are evaluated at 15 radial stations (starting from 0.25R to 0.95R with an increment of 0.05R) for each blade. Hence, there are in total 45 variables representing lift, drag and moment coefficients for one blade. It may be noted (from Eqs. 10-12) that there are four state variables for lift, two state variables each for drag and moment. Therefore, the total number of state variables representing the sectional aerodynamics for one blade is 120 (15 radial stations $\times$ 8 state variables per stations). The rotor blade structural model is represented by eight modes consisting of four flap modes, two lag modes, one torsion mode and one axial mode. Hence, the total number of state variables representing structural modes per blade is 16. The time varying inflow is given by three state variables. Therefore, for a four bladed rotor system, there are in total 547

state variables (480 aerodynamic state variables + 64 structural state variables + three state variables for dynamic wake effects). In the present study, a four bladed system with proper spacing in the azimuth angle is considered for the analysis. By solving the response of all the blades simultaneously, one can identify the difference in the response of the blades as they go around the azimuth. Since, the response and loads of all the blades are solved at every instant of time, the time varying hub loads and the time varying inflow (dynamic wake effects) can be captured.

6.1 Flow Chart and Algorithm

A propulsive trim procedure has been adopted to obtain the main rotor control angles, tail rotor collective angle, fuselage roll and pitch attitudes. A fourth order Runge-Kutta integration scheme with a time step $\Delta t = 0.0025$ sec., has been used for solving the differential equations. Flow chart for calculation of helicopter trim and rotor response is shown in the Fig. 2. The steps involved in the evaluation of trim and response using DSDW model (which is computationally intensive as compared to other four models) are described below. These steps get simplified appropriately while using the other four models, namely, QSUI, QSDR, QSDW and DSDR.

1. For a given data including flight condition, evaluate mean rotor inflow based on all-up weight.

2. Assume initial values for trim variables ($\theta_0, \theta_{1c}, \theta_{1s}, \theta_{0T}, \Theta$ and Φ) and initial conditions for blade response.

3. Knowing rotor inflow and blade response, obtain the sectional aerodynamic loads for all the blades, by solving the dynamic stall equations.

4. Then using the sectional blade loads, the response of individual blades and rotor inflow variables are obtained simultaneously for the next time step, using blade equations and dynamic wake equations respectively.

5. Next, by using the blade response and inflow, go to step 3. This iteration is performed for about 40-50 rotor revolutions till convergence in the blade response and inflow variables are obtained.

6. Using the converged blade response, blade root loads and hub loads are obtained.

7. Then transfer the mean values of rotor hub loads, loads from horizontal tail, vertical tail, tail rotor and fuselage to the CG to satisfy the trim equations (Eq. 17).

8. Evaluate improved trim variables using Newton-Raphson technique.

9. Go to step 2. The iterations are continued till convergence in trim variables achieved. The convergence criterion is based on satisfying the condition that the difference in each trim setting between two successive iterations must be less than 0.002%.

7 Results and Discussions

Using the solution technique described in previous section, helicopter trim and aeroelastic response of the rotor blades are analysed for different cases to bring out: (i) the effect of aerodynamic modeling and (ii) the influence of structural couplings due to blade pretwist. Two sets of results are presented in the following. One set of results pertains to untwisted straight blade and the other set of results corresponds to a pretwisted blade configuration. Even though the response of all the blades in the rotor system is evaluated independently, for conciseness, in the description of the results only the response and loads of blade-1 (reference blade) are presented. The geometric description of the helicopter is shown in Fig. 1. The main rotor blade is modeled as a soft-in plane hingeless rotor blade with eight elastic modes representing four flap, two lag, one torsion and one axial modes. The rotor system consists of four blades. The data used in the present study are given in Tables 1 and 2.

7.1 Untwisted Straight Blade

The rotating natural frequencies and mode shapes for a nonuniform straight blade are evaluated. Mode shapes corresponding to flap deformation can be seen in Fig. 3. Mode shapes of lag, torsional and axial deformation can be seen in Fig. 4.

Using the five different aerodynamic models (QSUI, QSDR, QSDW, DSDR and DSDW), helicopter trim and blade response are evaluated for different forward speed conditions. The variation of control angles ($\theta_0, \theta_{1c}, \theta_{1s}, \theta_{0T}$) and the fuselage attitude in pitch (Θ) and roll (Φ) with forward speed are shown in Fig. 5. From Fig. 5a, it can be seen that the magnitude of the collective pitch angle (θ_0) is affected by the aerodynamic models used in the analysis. However, at high forward speeds ($\mu > 0.25$), the aerodynamic models do not significantly influence the collective pitch angle. It is observed that the models with dynamic wake (QSDW and DSDW) require high collective pitch setting at low forward speeds than the other aerodynamic models. For hover, the variation in the collective pitch angle for all these models is of the order 0.75 deg. A similar observation can be made for the tail rotor collective pitch (θ_{0T}) as shown in Fig. 5d.

The variation of the lateral cyclic control angle (θ_{1c}) with forward speed is shown in Fig. 5b. From the figure, it can be seen that inclusion of Drees model with quasi-steady aerodynamics (QSDR) increases the control angle in the transition zone (*i.e.*, in the range $\mu = 0.05$ to 0.075). The increase is more pronounced if dynamic wake model is used (QSDW) instead of Drees model. In this transition zone, dynamic stall model has very little effect but as μ increases dynamic stall model shows more reduction in control angle as compared to quasi-steady aerodynamics. This type of sharp rise and fall in the variation of θ_{1c} obtained with DSDW model qualitatively resembles the flight data presented in Ref. [32] (shown in Fig. 6). Dynamic stall models require more longitudinal cyclic control angle (θ_{1s}) at high forward speeds as can be seen in Fig. 5c. The equilibrium roll angle of the helicopter (as observed in Fig. 5e) is larger for QSUI model as compared to other four aerodynamic models. The equilibrium roll angle is the least for the two dynamic wake models DSDW and QSDW;

and the roll angles are found to be almost the same for these two models. It is interesting to note from Fig. 5f that the pitch attitude of the helicopter shows a monotonic increase with forward speed; but at high forward speeds there is a slight reduction in the pitch angle for the two dynamic stall models DSDR and DSDW.

The reason for the observed sharp rise and fall in lateral cyclic control angle as shown in Fig. 5b, can be explained by analyzing the inflow variables. For the sake of comparison, a new set of common inflow parameters λ_0, λ_{1c} and λ_{1s} has been introduced. In Drees model, these parameters denote $\lambda_0 = \lambda_i$, $\lambda_{1c} = \lambda_i k_y$ and $\lambda_{1s} = \lambda_i k_x$. In the dynamic wake model, the parameters are equal to $\lambda_0 = \sqrt{3}\ \alpha_1^0$, $\lambda_{1c} = \sqrt{15/2}\ \alpha_2^1$ and $\lambda_{1s} = \sqrt{15/2}\ \beta_2^1$. Figure 7 shows the variation of inflow variables for DSDR and DSDW models, in the transition zone ($\mu = 0.075$). The collective inflow (λ_0) predicted by the two models are close to each other and it is around 0.04. The lateral variation of inflow (λ_{1s}) is one order smaller than the longitudinal (λ_{1c}) and collective inflow quantities. Dynamic wake model (DSDW) predicts the longitudinal inflow as $\lambda_{1c} = 0.055$, which is much higher than that predicted by Drees model DSDR (λ_{1c}=0.03). Because of the high value of λ_{1c}, a high value of θ_{1c} is required for equilibrium with DSDW model as compared to DSDR model. The inflow variables at high forward speed ($\mu = 0.3$) are shown in Fig. 8 for DSDR and DSDW models. The collective inflow λ_0 predicted by the two models are almost equal and it is around 0.01. Lateral variation of inflow λ_{1s} is one order smaller than λ_0 and λ_{1c}. The inflow variable λ_{1c} is reduced as compared to the values obtained for $\mu = 0.075$. Because of the reduction in the value of λ_{1c} at high forward speeds, the lateral cyclic control angle also shows a reduction at high speeds as can be seen in Fig. 5b.

The harmonic contents of hub vertical load T are shown in Fig. 9. From Fig. 9a, it is observed that the amplitude of the 4/rev frequency (20 Hz) is around 810 N for DSDW model and it is only about 100 N for QSUI model. The enlarged figure (Fig. 9b) show that DSDW model provides a large number of harmonics including those below 20 Hz (4/rev) in all the hub loads. From these figures, it is interesting to note that even QSUI model

predicts the presence of frequencies below 20 Hz (4/rev). This observation on the presence of a wide spectrum of frequencies in the hub loads is mainly due to the nonlinearity and the asymmetry associated with the aerodynamic models.

7.2 Effect of Structural Coupling due to Pretwist

The purpose of this study is to analyse the effects of structural coupling due to blade pretwist on helicopter trim, and aeroelastic response of the rotor blade and hub loads. Four different values of pretwist, namely -4 deg., -8 deg., -12 deg. and -16 deg. are considered. In all these configurations, the tip pitch angle is set at 4 deg. For example, for a blade configuration with -8 deg. pretwist, if the control pitch input is zero, then the root pitch angle of the blade is 12 deg. and the tip pitch angle is 4 deg. Mode shapes for -8 deg. twisted blade configuration are generated and are shown in Figs. 10 and 11. From the figures, it is evident that the twist introduces coupling in flap and lag modes. The contribution of lag in first flap mode is close to 6% (Fig. 10), whereas contribution of the flap in first lag mode is less than 1% (Fig. 11). The aeroelastic analysis is performed using the DSDW aerodynamic model. In the following, a comparison of trim results for straight and -8 deg. twisted blade configurations, is presented.

The variation of control angles ($\theta_0, \theta_{1c}, \theta_{1s}, \theta_{0T}$) and the fuselage attitude in pitch (Θ) and roll (Φ) with forward speed are shown in Fig. 12. The trend of all the control angles is similar for both cases of straight and twisted blade configurations. From Fig. 12a, it is evident that the magnitude of the collective pitch angle (θ_0) is low in the case of twisted blade as compared to the straight blade. The difference of about 6 deg. in collective pitch essentially corresponds to the pitch of the pretwisted blade at 75% radial location. The observed dip in the fuselage pitch attitude at the high advance ratio for the straight blade configuration is eliminated in the case of the twisted blade configuration (Fig. 12f).

The variation of hub loads for one revolution is shown in Fig. 13 for the various twisted blade configurations (-4, -8, -12 and -16 deg.), for an advance ratio $\mu = 0.35$. It can be seen

that the mean values of longitudinal force (H) (Fig. 13(a)), lateral force (Y) (Fig. 13(b)) and yawing moment (Mz) (Fig. 13(f)) differ by a significant amount for the twisted and untwisted blade configurations. The reduction in the value of mean yaw moment is responsible for the reduction in θ_{0T} (collective trim setting of tail rotor) for twisted blade configuration as compared to straight blade configuration. The mean values remain almost the same for thrust (T) (Fig. 13(c)), roll moment (Mx) (Fig. 13(d)) and pitch moment (My)(Fig. 13(e)) (except for -16 deg. pretwist). It is observed that blade pretwist reduces the amplitude of hub load variations. This observation can also be seen by comparing the magnitudes of harmonic contents in thrust (T), shown in Fig. 9 (for straight blade configuration with DSDW model) and Fig. 14 (for -8 deg. and -16 deg. twisted blade configuration with DSDW model). It can be seen from Fig. 14 that the magnitudes of the various harmonics corresponding to pretwisted blade are smaller than those obtained for straight blade. The amplitude of 4/rev frequency (20 Hz) is found to be 650 N and 560 N for the -8 deg. and -16 deg. twisted blade respectively and for the straight blade the value is 810 N.

Sectional aerodynamic lift, moment and drag at various radial stations (50%R, 65%R, 75%R, 85%R and 95%R) are shown respectively in Figs. 15-17, for one blade as it goes around the azimuth, for an advance ratio $\mu = 0.35$. From Fig. 15, it can be seen that for the case of straight blade configuration, the minimum value of the sectional lift force is almost the same in both advancing and retreating sides at all the radial stations. Whereas, for the case of twisted blade configuration, the occurrence of minimum value of the sectional lift force shifts from retreating side to advancing side as the radial station moves towards the tip. From Fig. 16, it is observed that the sectional moment shows identical variation at in-board sections (50%R and 65%R) for both twisted and straight blade configurations. At the out-board stations (85%R and 95%R), the sectional moment undergoes a large variation in the retreating side for the straight blade as compared to the twisted blade configuration. From Fig. 17, it is observed that at the out-board stations (85%R and 95%R), the variation in sectional drag force is considerably small for the twisted blade configuration as compared

to straight blade configuration. These results show that the effect of dynamic stall is reduced in the retreating side due to blade pretwist.

The tip response of a single blade in flap, lag and torsional modes is shown in Fig. 18. The magnitude of the variation of the tip response is relatively small for the case of twisted blade configuration as compared to the straight blade configuration. Figure 18 shows that the torsional response has more harmonics as compared to flap and lag response. Variation in pretwist seems to have more influence on flap and lag deformations, as compared to torsional deformation. Mean value of flap and lag deformations decrease with increase in pretwist upto a value of -12 deg. and then it increases for -16 deg. pretwist.

The variation of root loads for a single blade as it goes around the azimuth is shown in Fig. 19. From the figure, it can be seen that there is a reduction in the magnitudes of the root loads for the case of twisted blade configuration as compared to the straight blade configuration.

Various harmonics of the blade root loads are shown in Fig. 20. This figure shows several interesting features. Inclusion of pretwist reduces all the harmonic contents for the root loads F_{x1k}, F_{y1k} and M_{z1k} (*i.e.*, Figs. 20(a), 20(b) and 20(f)). For the case of vertical root shear F_{z1k} (Fig. 20(c)), $1/rev$ component shows an increase with increase in pretwist and all the other components show a reduction with increase in pretwist. For the case of root torsional moment M_{x1k} (Fig. 20(d)), -8 deg. pretwist provides a minimum value of $1/rev$ and $2/rev$ componets, whereas inclusion of twist shows a monotonic reduction in higher harmonic components. In the case of root flap moment M_{y1k} (Fig. 20(e)), there is no appreciable change in $1/rev$ component, whereas there is a reduction in other harmonic contents with inclusion of pretwist.

8 Concluding Remarks

A computational aeroelastic model has been developed, wherein the equations representing the blade dynamics, rotor inflow and sectional aerodynamics including stall are solved in a

sequential manner. A four bladed system with proper spacing in the azimuth angle has been considered for the analysis. By solving simultaneously the response of all the blades, one can identify the difference in the response of the blades as they go around the azimuth. Since the response and loads of all the blades are solved at every instant of time, the time varying hub loads and time varying inflow (dynamic wake effects) can be captured. A systematic study is undertaken to analyse the influence of five different aerodynamic models and the effect of pretwist on the helicopter trim and aeroelastic response of the rotor blades.

The important observations of this study can be summarised as:

1. The lateral cyclic pitch (θ_{1c}) setting required for trim is significantly affected by rotor inflow at low forward speeds ($0 < \mu < 0.1$), and by dynamic stall effects at forward speeds ($\mu > 0.15$). It is also found that the aerodynamic model, incorporating dynamic wake and dynamic stall effects, predicts the trim parameter (θ_{1c}) whose variation with forward speed resembles closely to those obtained in flight test.

2. The structural coupling due to blade pretwist is observed to significantly alter the time variation of the sectional loads as compared to the loads obtained for a straight untwisted blade. This result indicates that aeroelastic couplings have a significant influence on the rotor loads.

9 Acknowledgment

The authors acknowledge the financial support provided by DST India.

Table 1: Helicopter data

Variable		Quantity
Number of blades,	N_b	4
Air density at sea level,	$\rho\ (kg/m^3)$	1.224
Weight of the Helicopter,	$W\ (N)$	45000
Radius of the main rotor blade,	$R\ (m)$	6.6
Radius of the tail rotor blade,	$R_t\ (m)$	1.3
Chord of the main rotor blade,	$C\ (m)$	0.5
Chord of the tail rotor blade,	$C_t\ (m)$	0.19
Main rotor rotating speed,	$\Omega\ (rpm)$	300
Tail rotor rotating speed,	$\Omega_t\ (rpm)$	1500
Fuselage frontal area,	$f\ (m^2)$	1.8
Horizontal tail area,	$s_h\ (m^2)$	2.24
Vertical tail area,	$s_v\ (m^2)$	2.126
Blade Frequency data (Untwisted): Nondimensional		
Flap modes		1.089
		2.896
		5.145
		7.688
Lag modes		0.701
		5.308
Torsional mode		4.509
Axial mode		9.155
Blade Frequency data (-8 deg. twist): Nondimensional		
Flap modes		1.093
		2.822
		4.865
		7.150
Lag modes		0.701
		5.293
Torsional mode		4.508
Axial mode		9.155

Table 2: Geometrical data of the helicopter

Variable	Quantity (m)
X_{MR}	0.0
X_{HT}	7.5
X_{VT}	7.5
X_{TR}	7.5
Y_{MR}	0.0
Y_{HT}	0.0
Y_{VT}	0.0
Y_{TR}	0.0
Z_{MR}	2.0
Z_{HT}	0.5
Z_{VT}	1.75
Z_{TR}	2.0

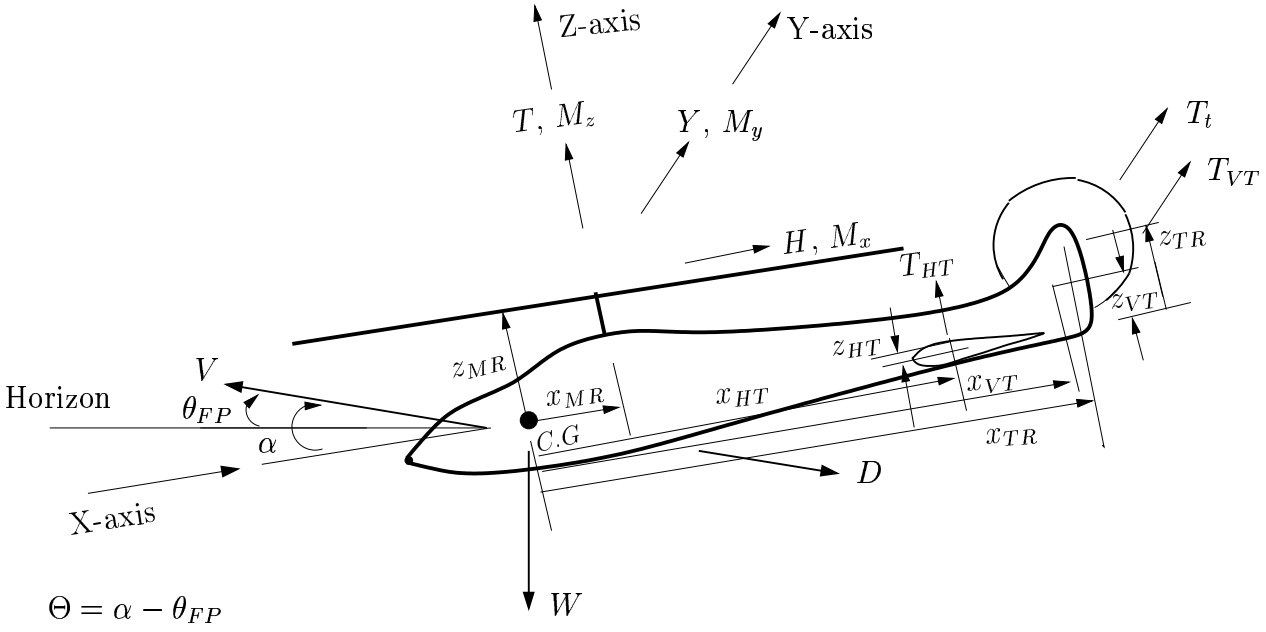

(a) Side view

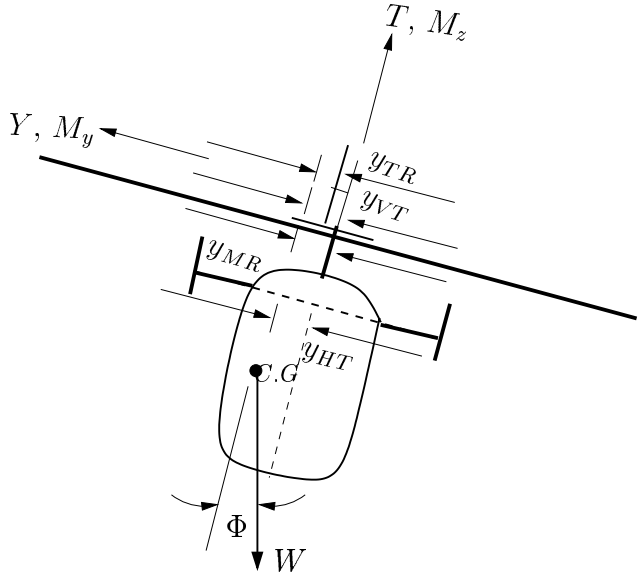

(b) Front view

Figure 1: Loads and orientation of the helicopter

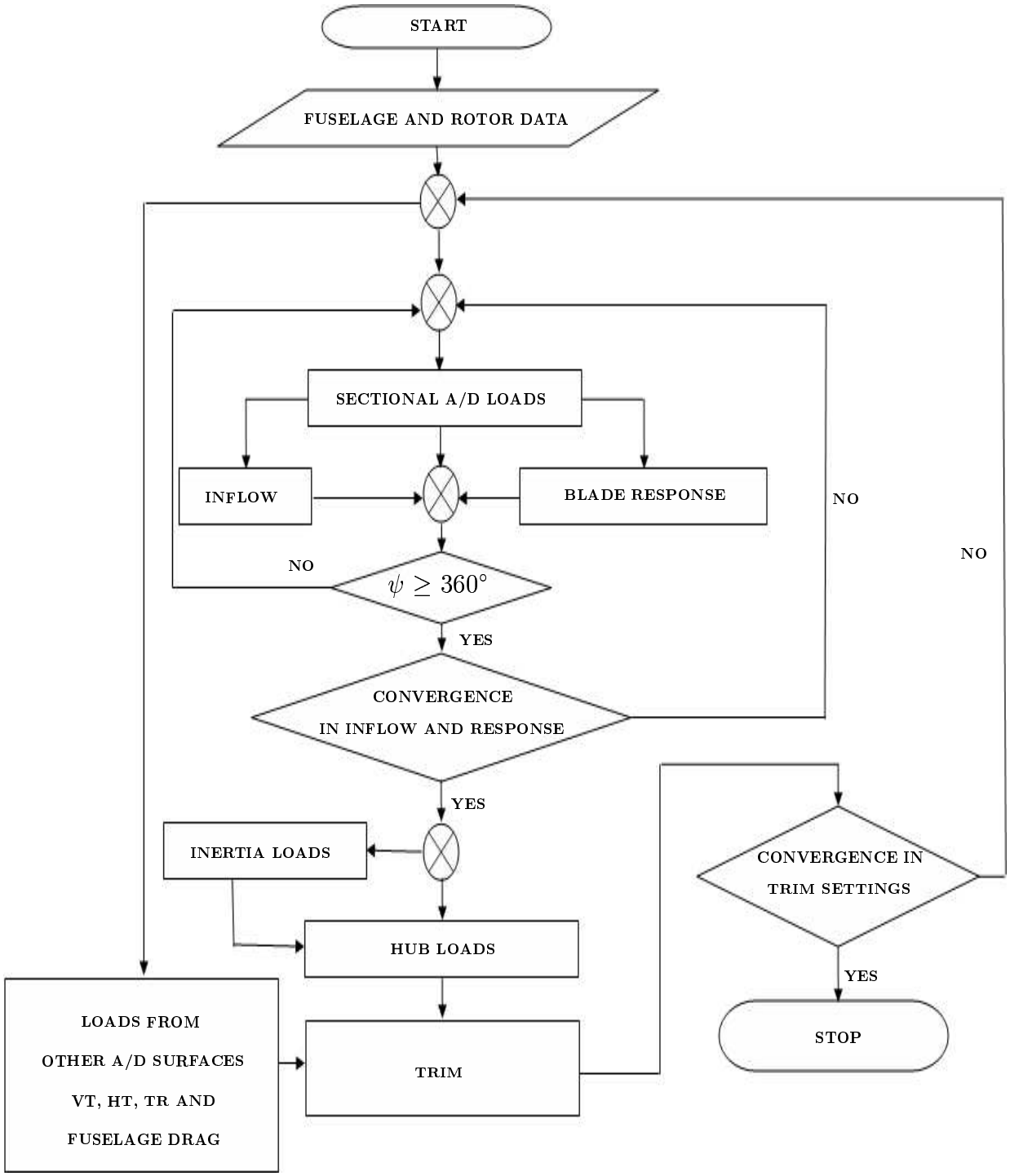

VT — Vertical Tail; HT — Horizontal Tail; TR — Tail Rotor

Figure 2: Flow chart for calculation of helicopter trim and rotor response

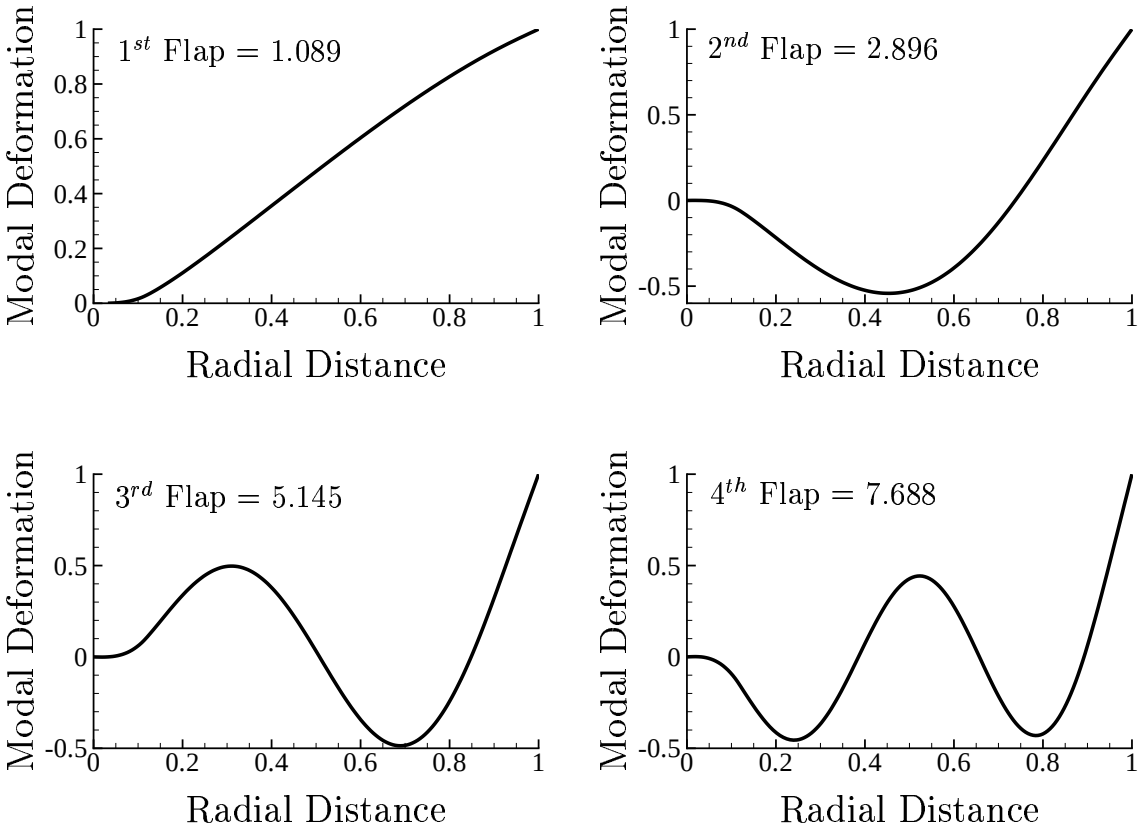

Figure 3: Mode shapes of straight blade in flap (out-of-plane bending) mode (nondimensional)

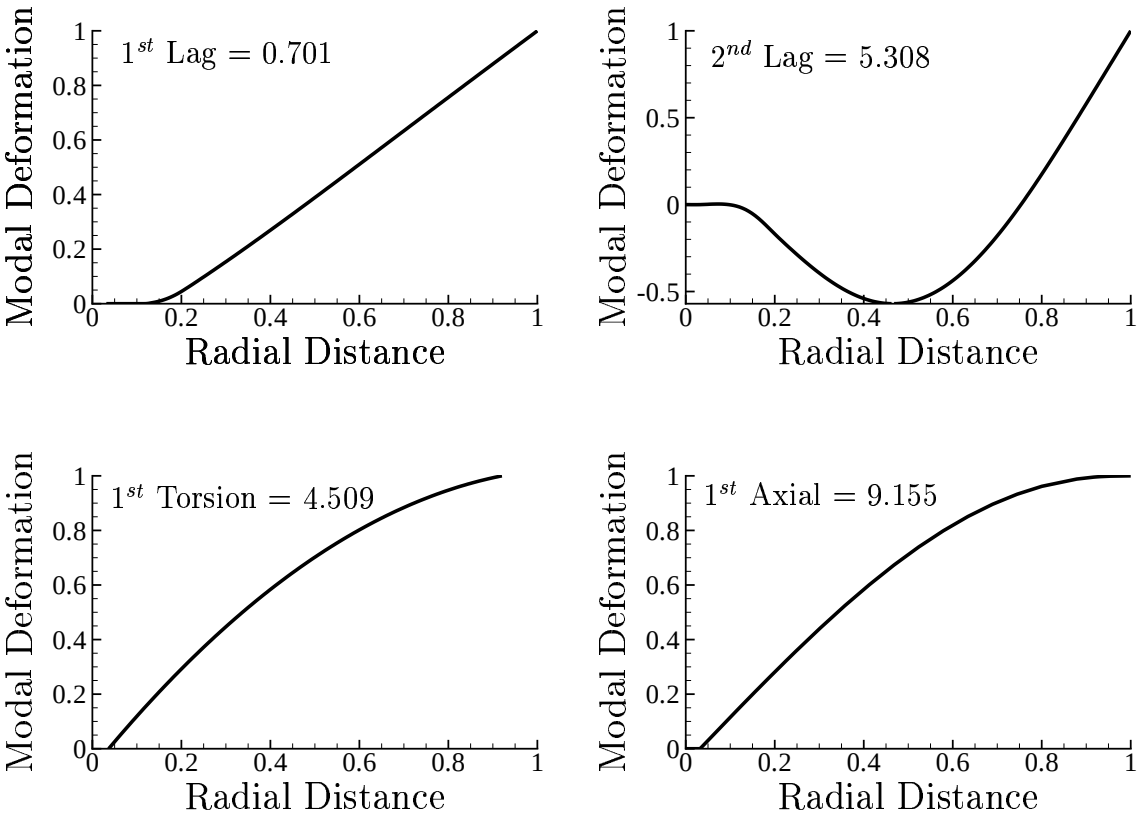

Figure 4: Mode shapes of straight blade in lead-lag (in-plane bending), torsional and axial mode (nondimensional)

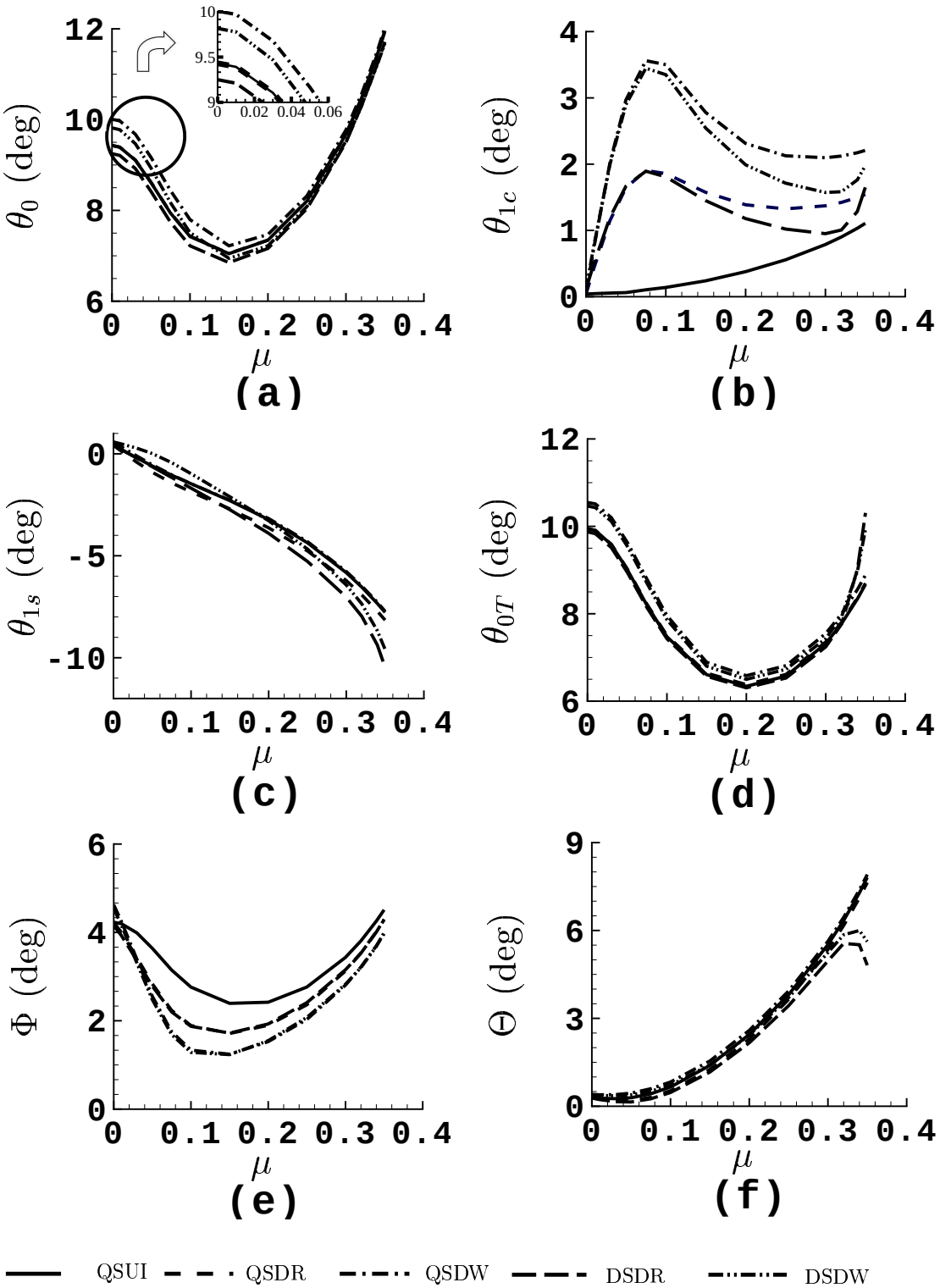

Figure 5: Variation of trim angles with forward speed μ

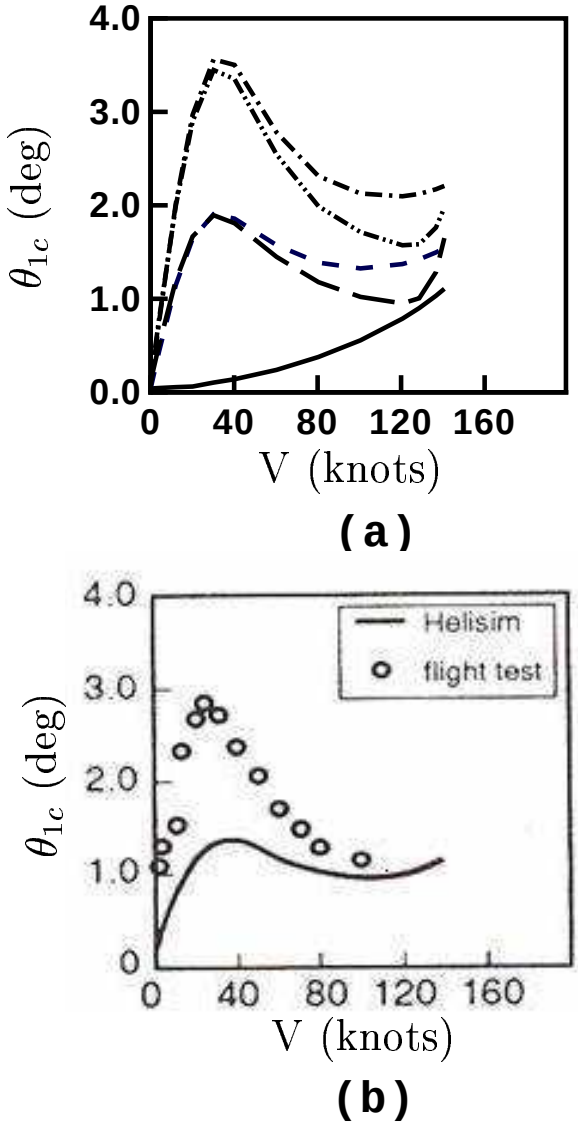

Figure 6: Qualitative comparison of variation of lateral pitch angle with forward speed (a) present study (b) Ref. [32]

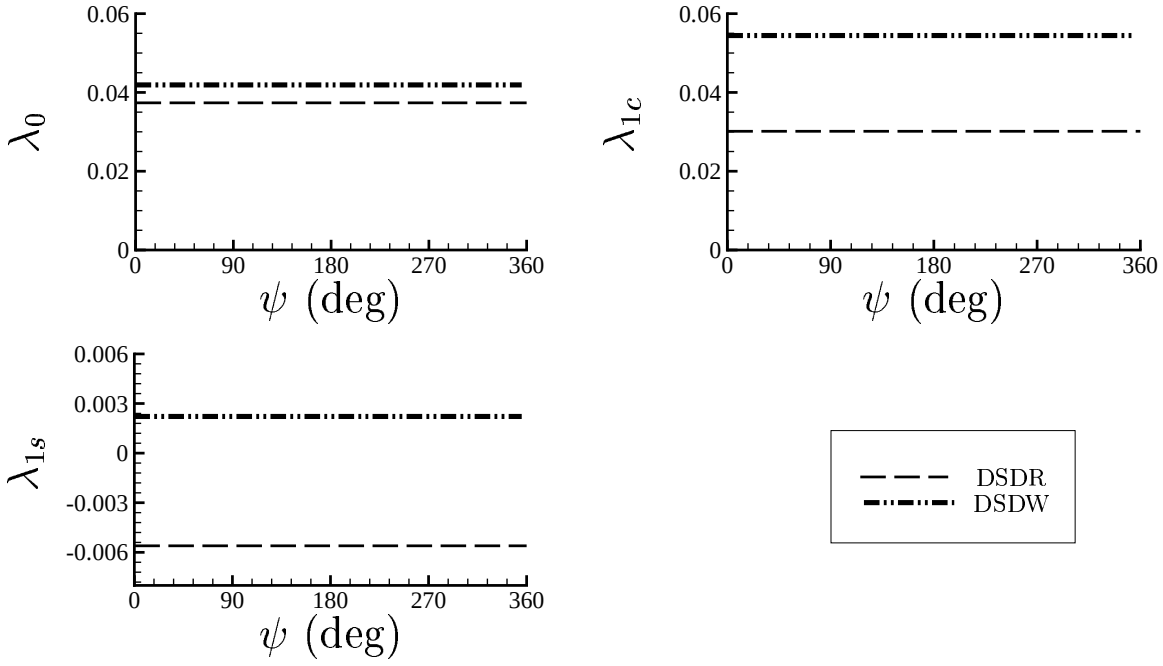

Figure 7: Comparison of inflow variables for Drees and dynamic wake models as a function of azimuth for $\mu = 0.075$

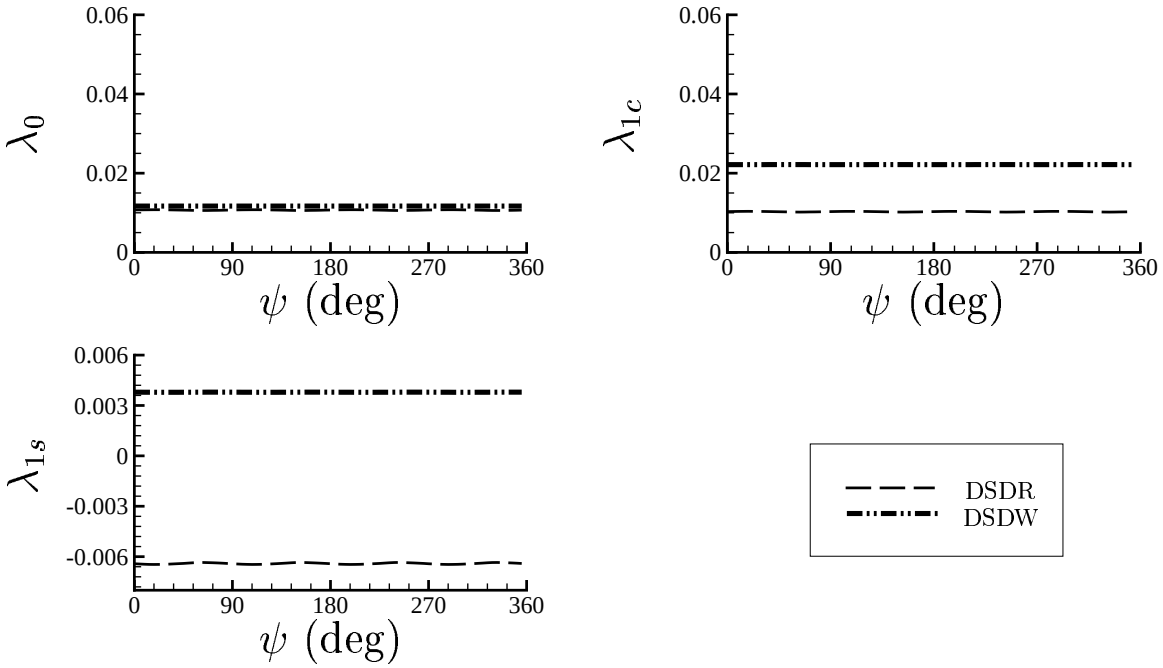

Figure 8: Comparison of inflow variables for Drees and dynamic wake models as a function of azimuth for $\mu = 0.30$

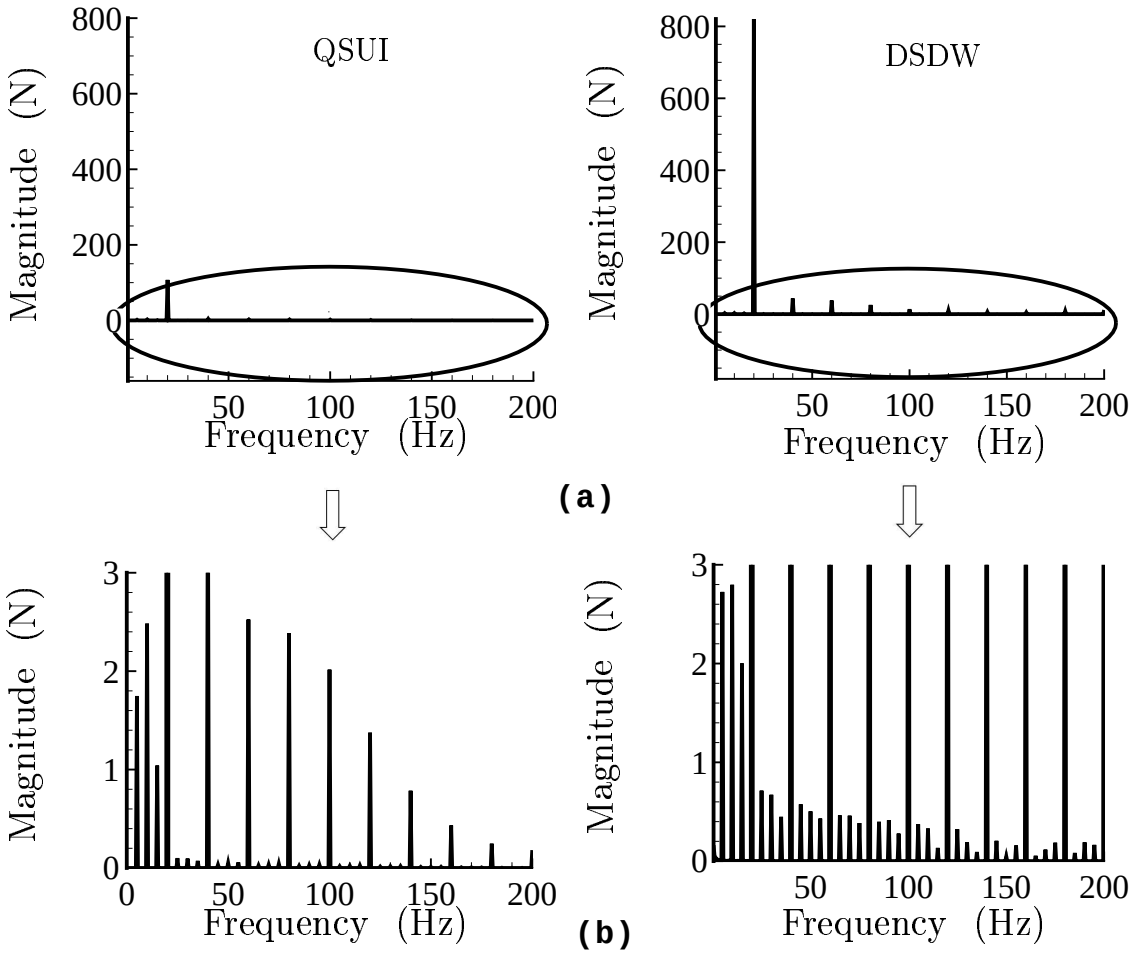

Figure 9: Frequency contents of vertical force (T) at the hub for $\mu = 0.35$

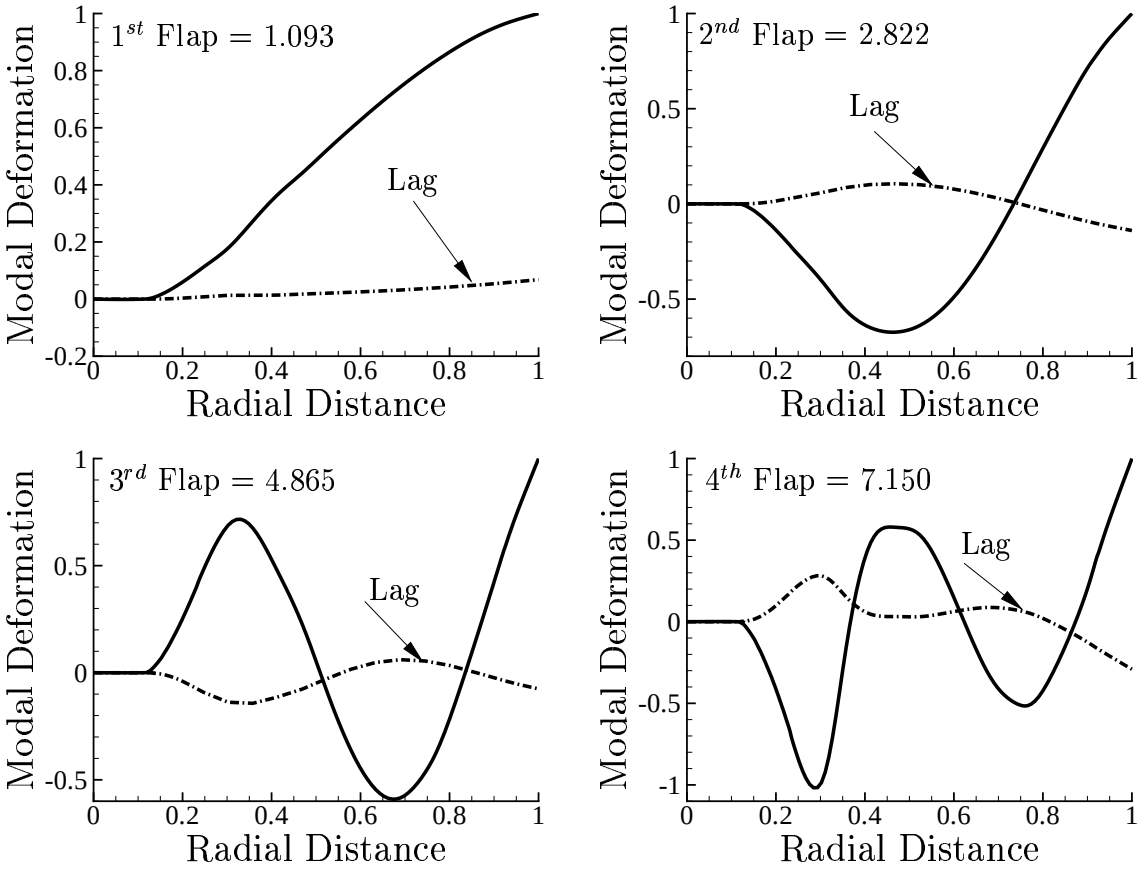

Figure 10: Mode shapes of twisted blade in coupled flap (out-of-plane bending) mode (nondimensional)

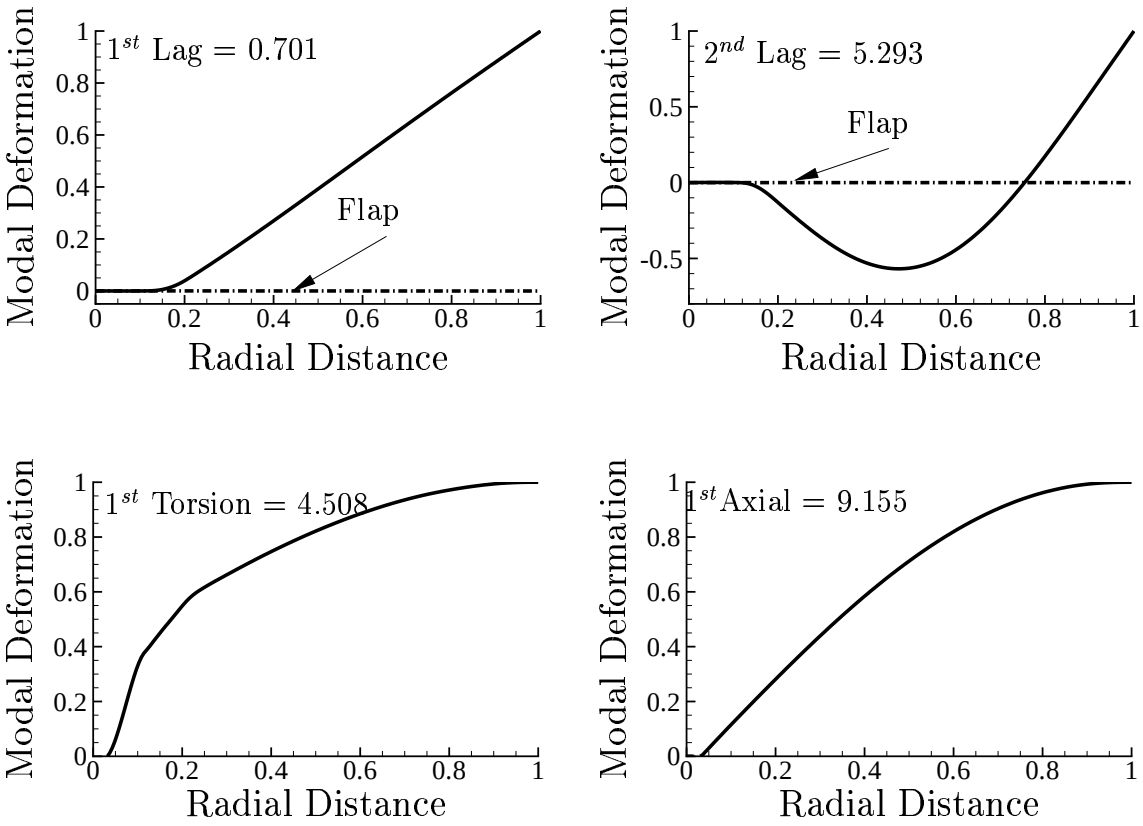

Figure 11: Mode shapes of twisted blade in coupled lead-lag (in-plane bending), torsional and axial mode (nondimensional)

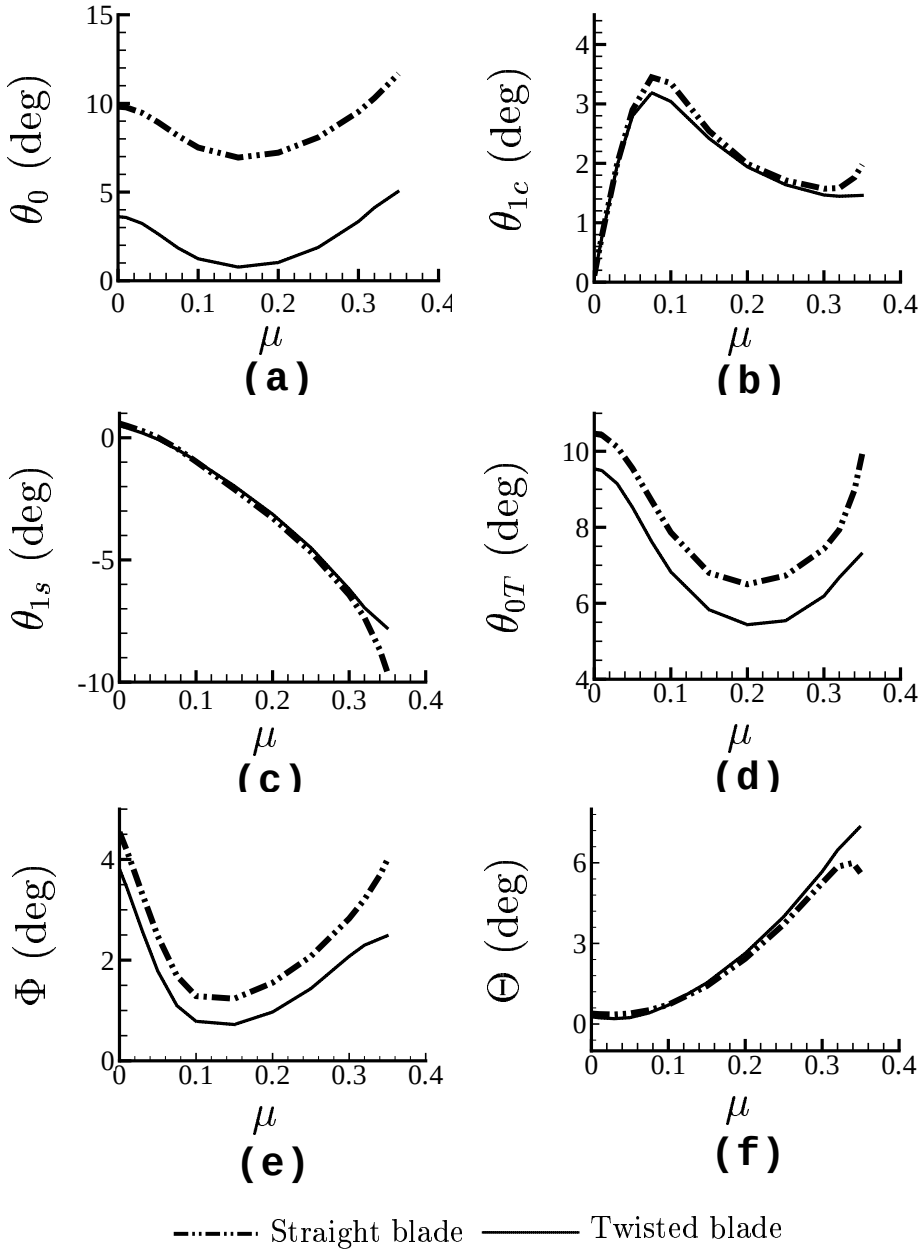

Figure 12: Trim variables for twisted and straight blade configuration as a function of advance ratio (μ) obtained using DSDW model

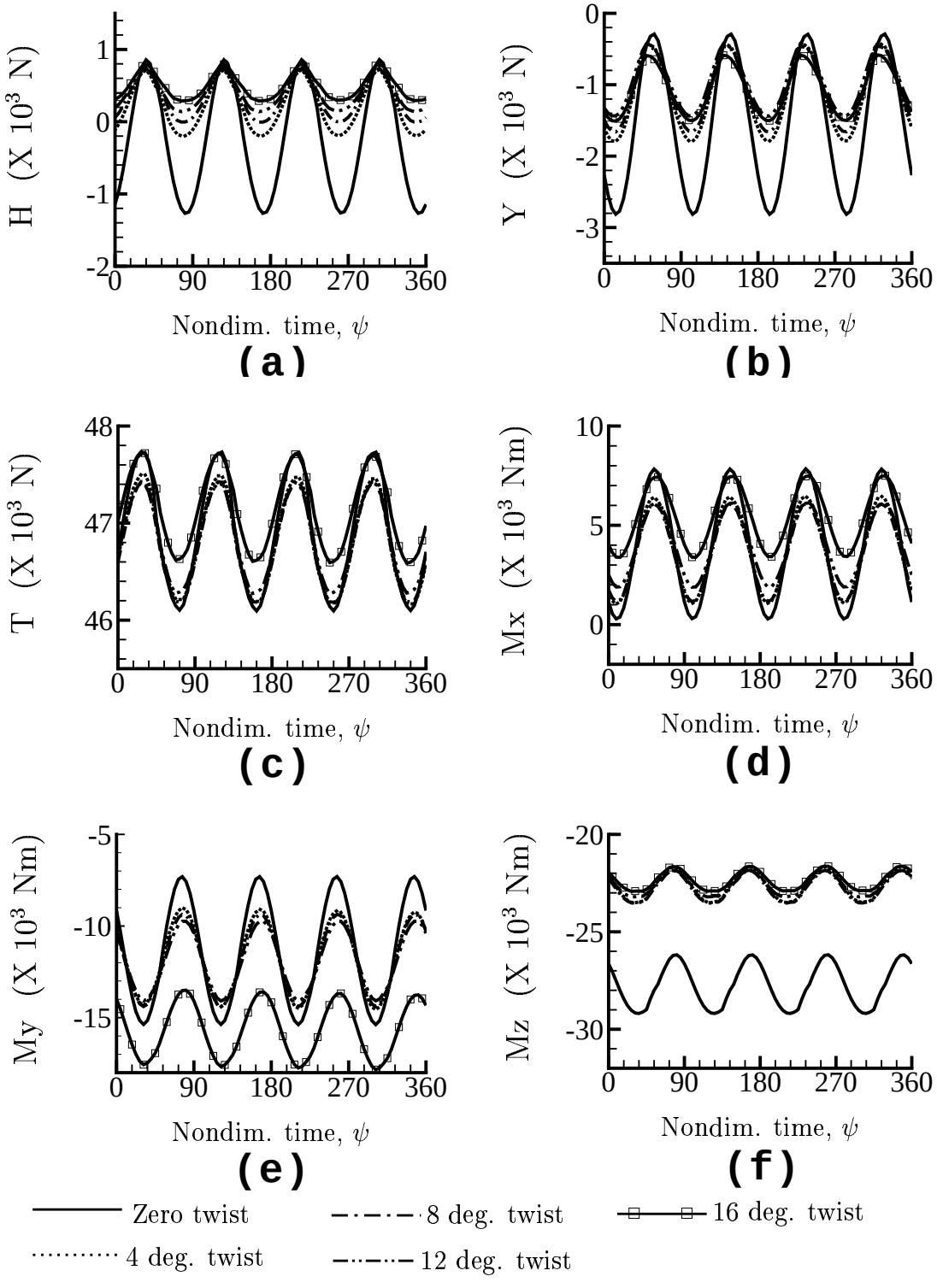

Figure 13: Comparison of hub loads for twisted and straight blade configuration as a function of azimuth for $\mu = 0.35$ obtained using DSDW model

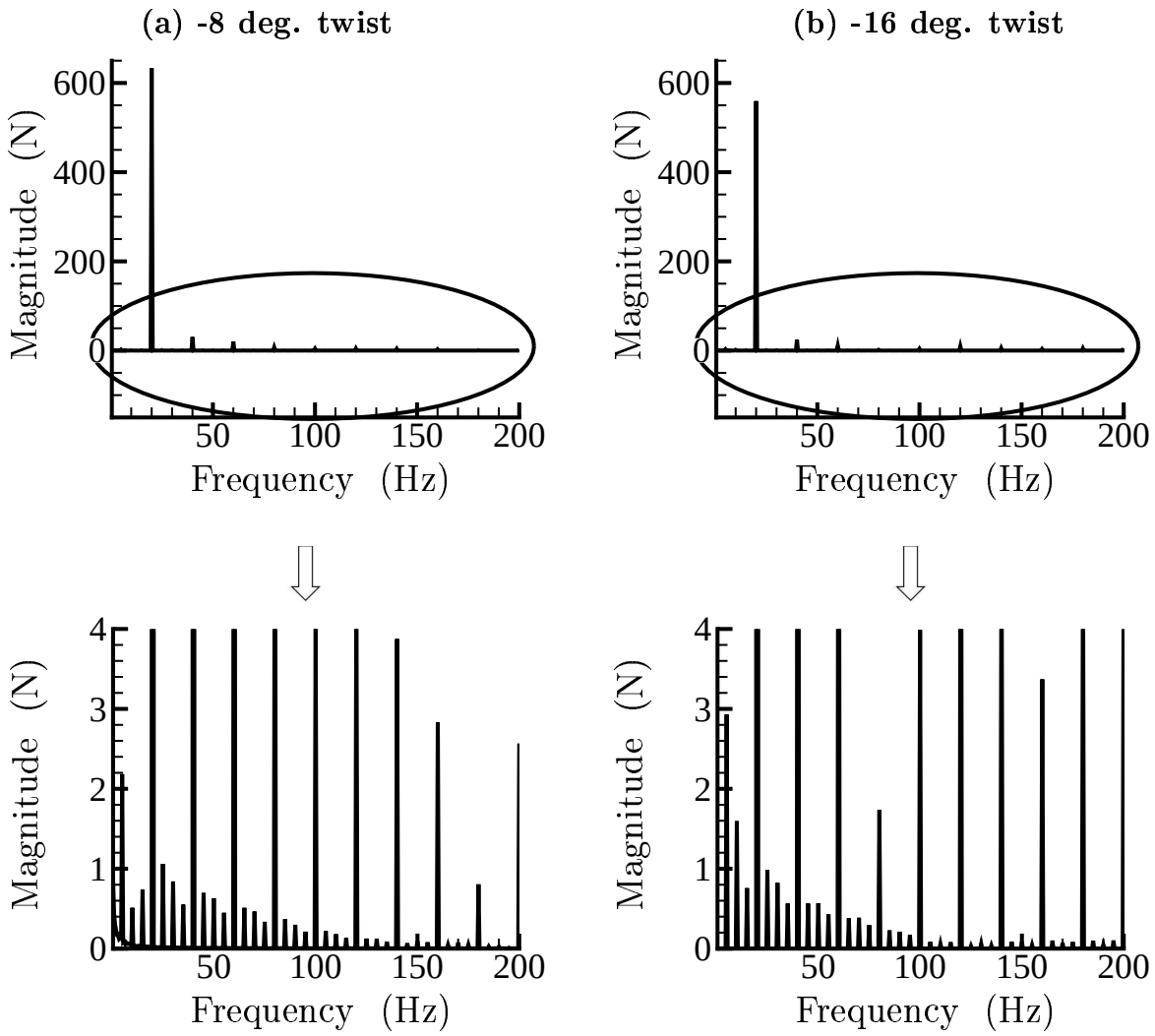

Figure 14: Frequency contents of vertical force at the hub obtained for twisted blade configuration for $\mu = 0.35$ obtained using DSDW model

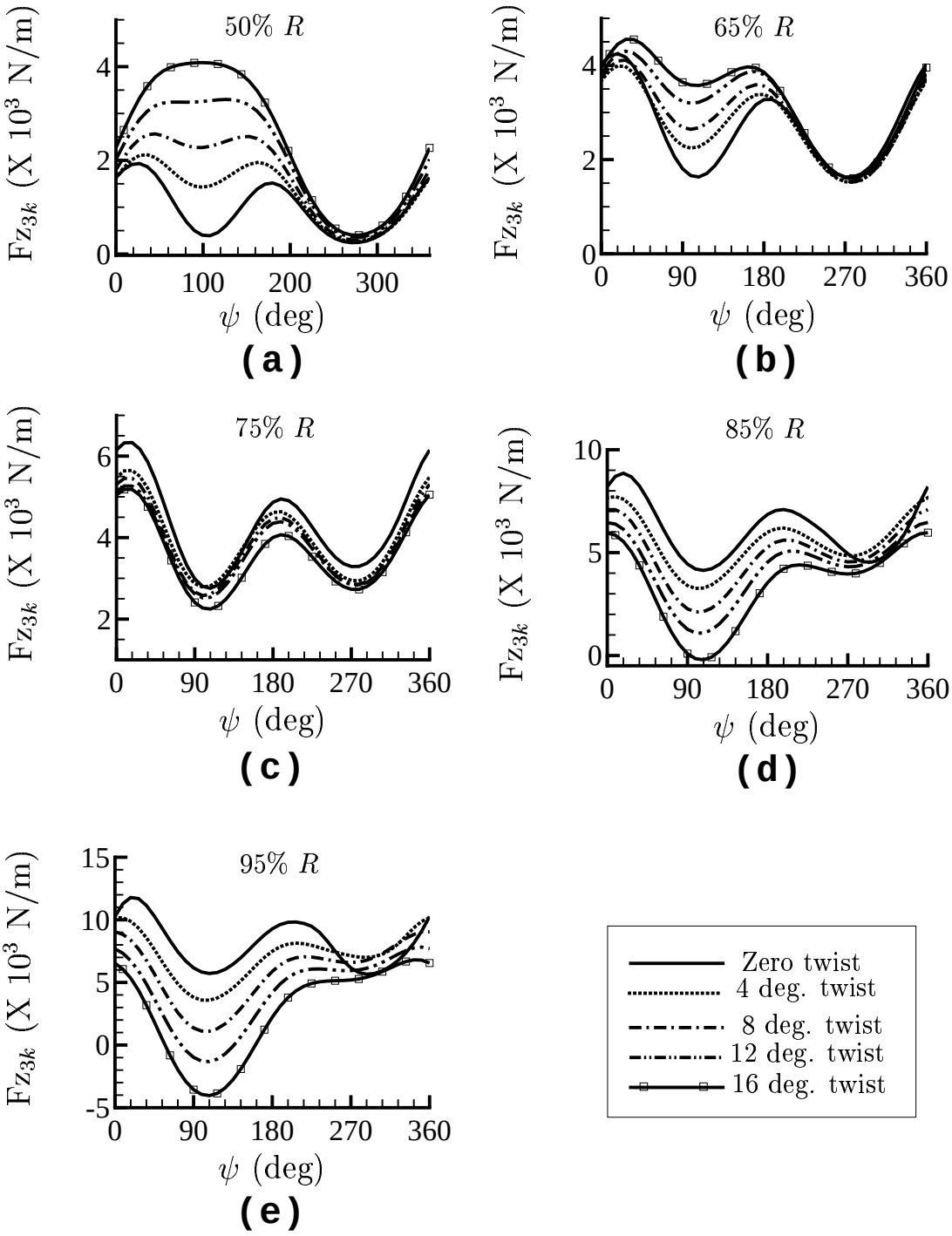

Figure 15: Comparison of sectional lift at various radial locations for twisted and straight blade configurations as a function of azimuth for $\mu = 0.35$, obtained using DSDW model

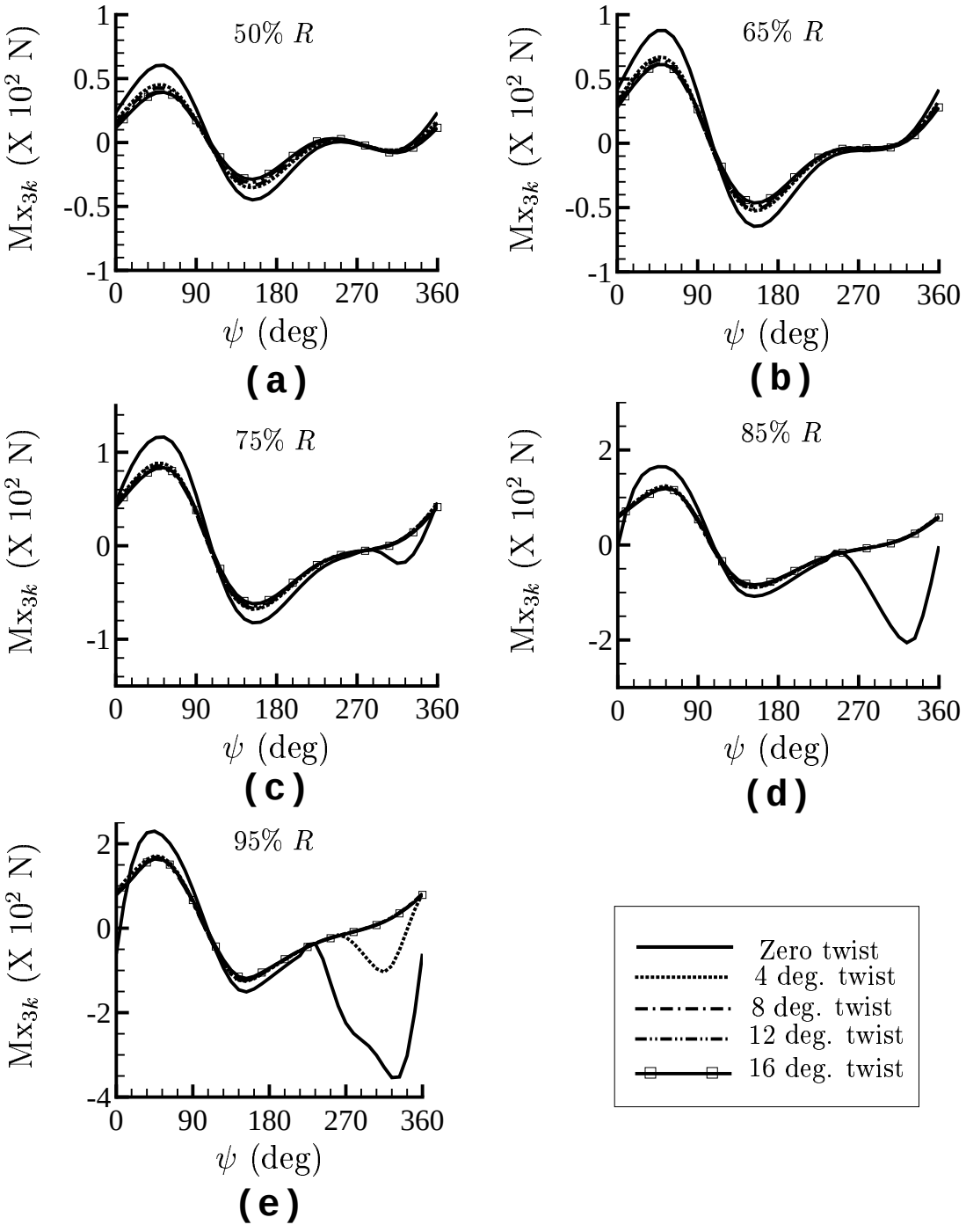

Figure 16: Comparison of sectional moment at various radial locations for twisted and straight blade configurations as a function of azimuth for $\mu = 0.35$, obtained using DSDW model

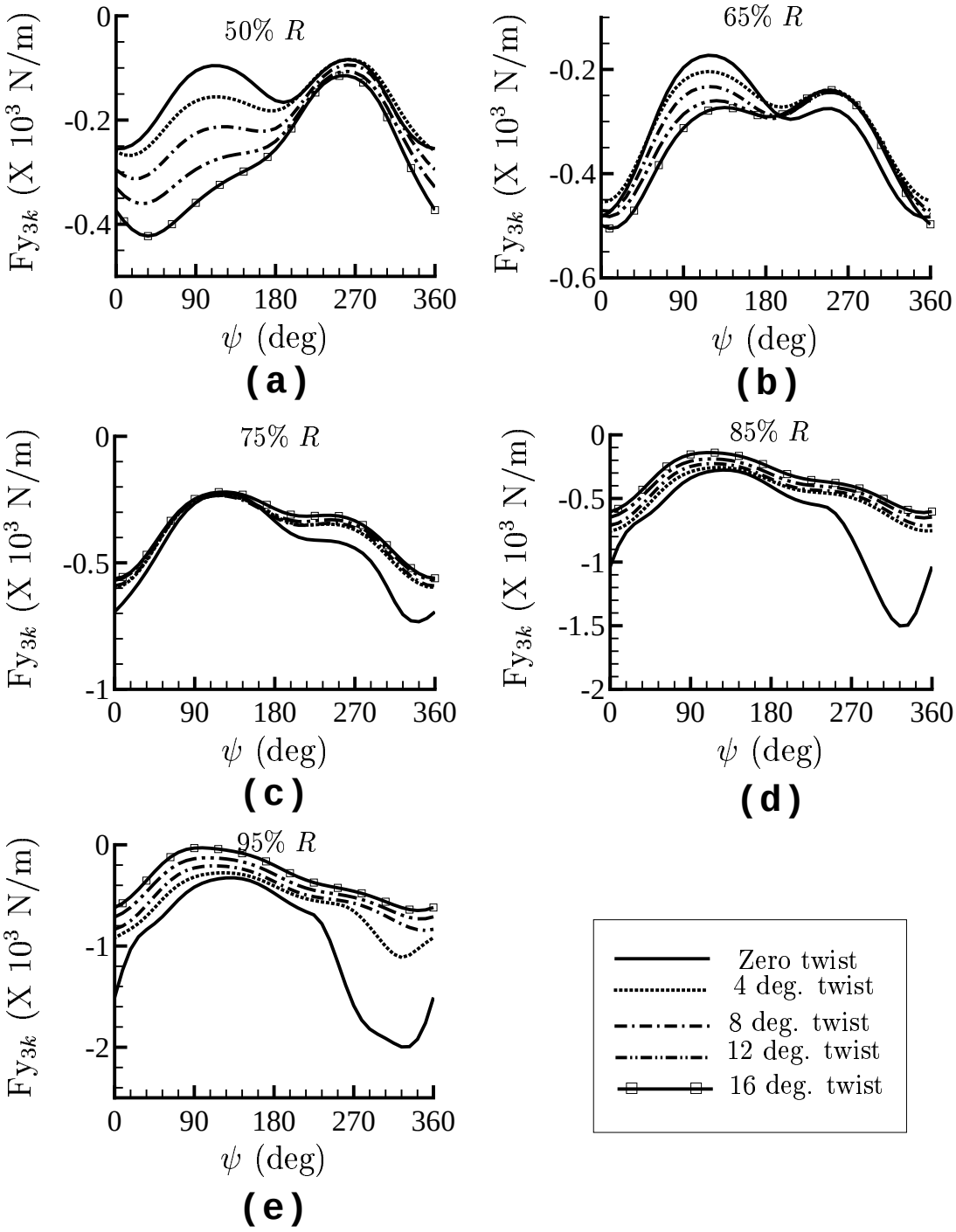

Figure 17: Comparison of sectional drag at various radial locations for twisted and straight blade configurations as a function of azimuth for $\mu = 0.35$, obtained using DSDW model

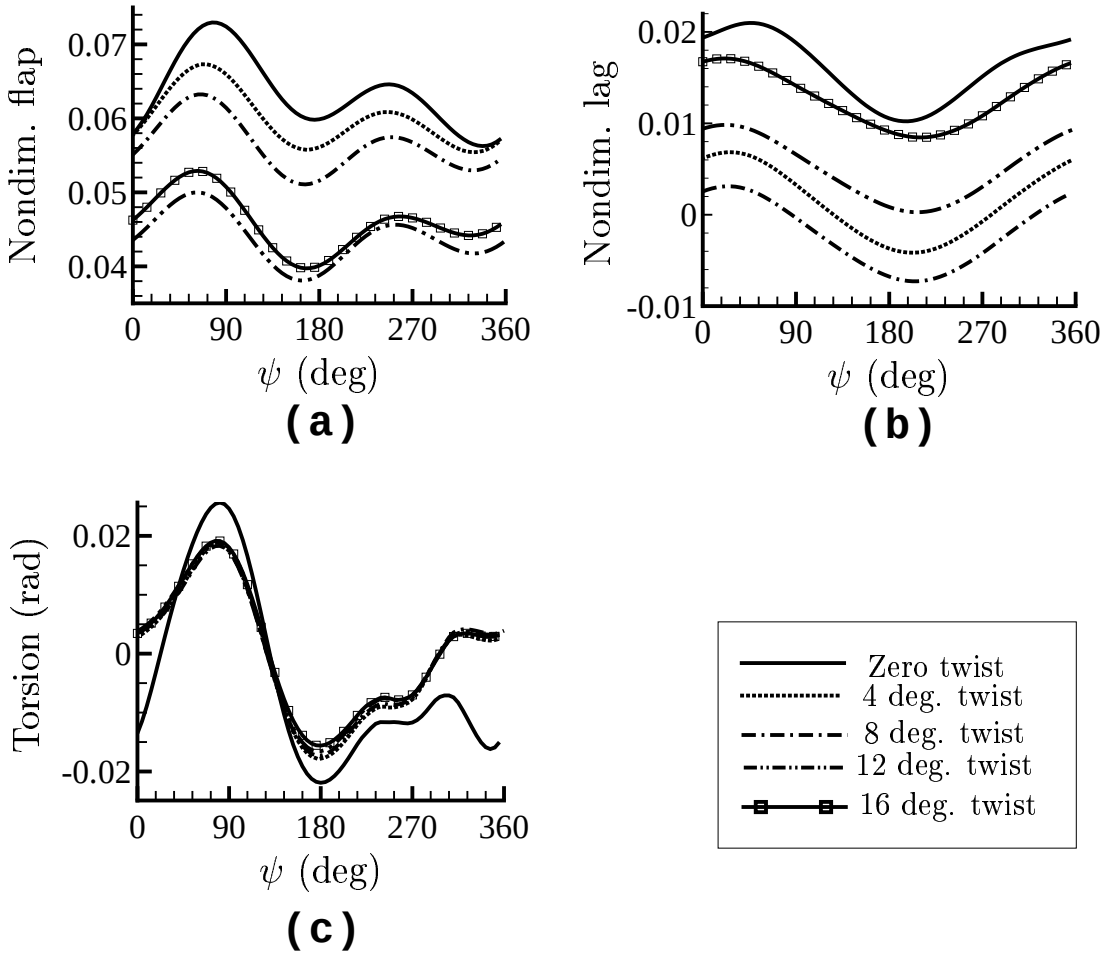

Figure 18: Comparison of tip deformations of the rotor blade for twisted and straight blade configurations as a function of azimuth for $\mu = 0.35$ obtained using DSDW model

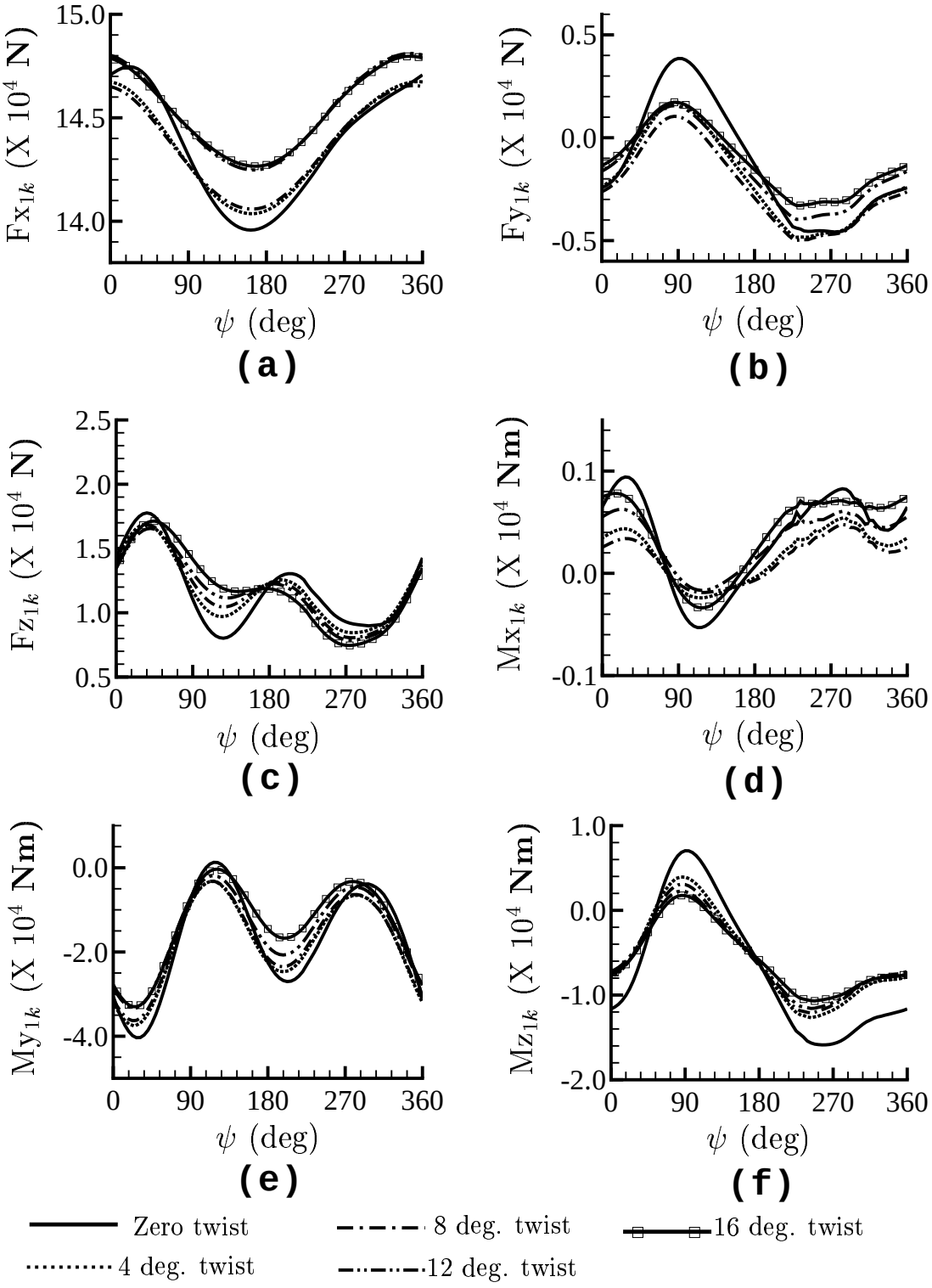

Figure 19: Comparison of root loads for twisted and straight blade configurations as a function of azimuth for $\mu = 0.35$ obtained using DSDW model

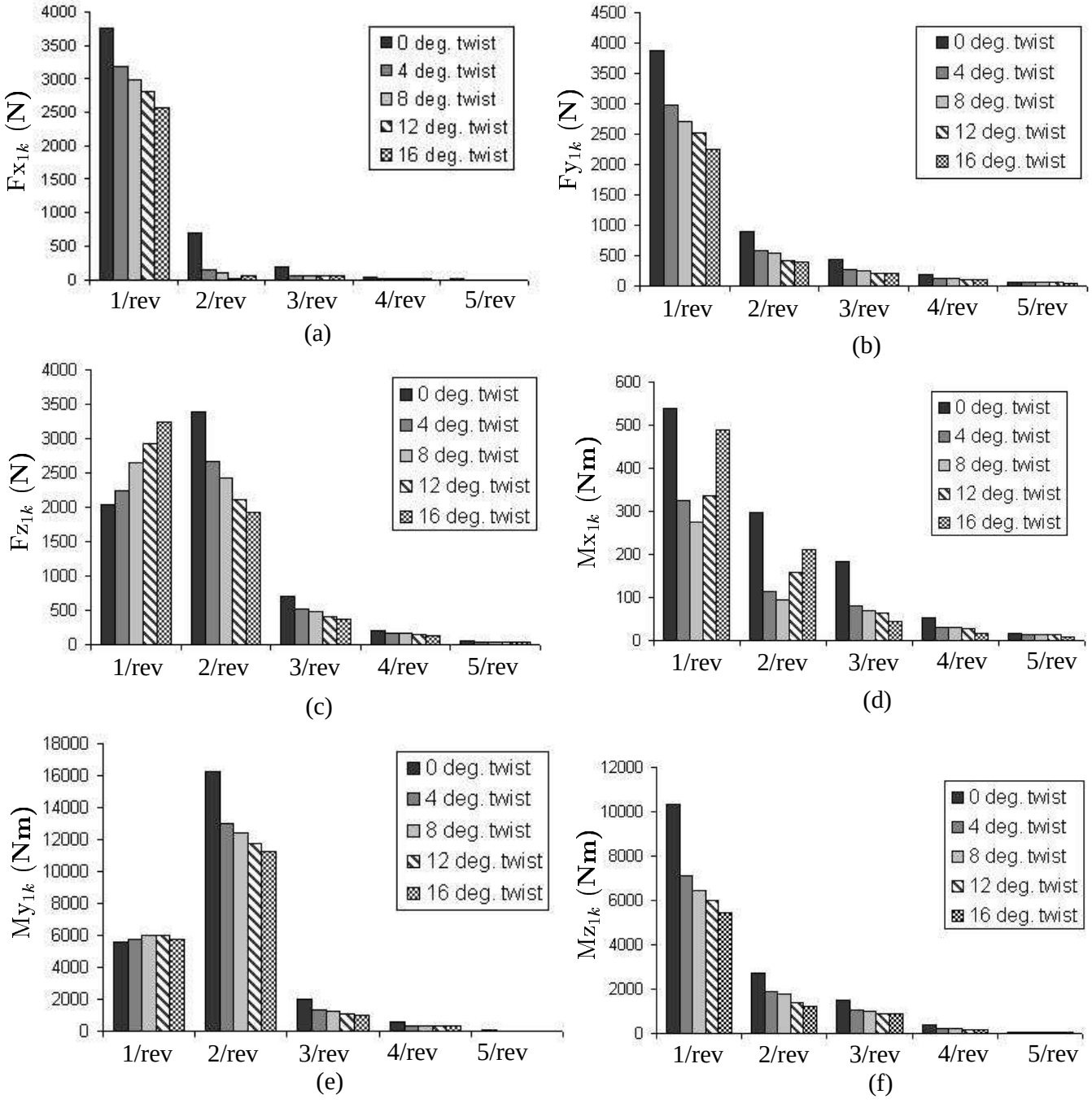

Figure 20: Harmonics of root loads for straight and twisted blade configurations obtained using DSDW model

References

[1] Friedmann, P. P., "Renaissance of Aeroelasticity and Its Future," *Journal of Aircraft*, Vol. 36, No. 1, 1999, pp. 105-121.

[2] Friedmann, P. P., and Hodges, D. H., "Rotary Wing Aeroelasticity — A Historical Perspective," *Journal of Aircraft*, Vol. 40, No. 6, 2003, pp. 1019-1046.

[3] Friedmann, P. P., "Rotary Wing Aeroelasticity: Current Status and Future Trends," *AIAA Journal*, Vol. 42, No. 10, 2004, pp. 1953-1972.

[4] Lytwyn, R. T., "An Analysis of the Divergent Vertical Helicopter Oscillations Resulting from the Physical Presence of the Pilot in the Collective Control Loop," *Proceedings of the* 22^{nd} *Annual Forum of the American Helicopter Society*, Washington, D.C., 1966.

[5] Bousman, W. G., "Putting the Aero Back Into Aeroelasticity," *Proceedings of the* 8^{th} *Annual Workshop on Aeroelasticity of Rotorcraft Systems*, University Park, PA, USA, 1999.

[6] Prasad, C. G. N., Dwivedi, V., and Dutta, R., "Vibration Monitoring in Helicopter Structure Using Rotor Noise: Flight Test Results and Discussions," *Proceedings of the* 15^{th} *National Seminar on Aerospace Structure*, Shree Maruthi Publishers, Coimbatore, India, 2007, pp. 161-165.

[7] Roget, B., and Chopra, I., "Individual Blade Control Methodology for a Rotor with Dissimilar Blades," *Journal of the American Helicopter Society*, Vol. 48, No. 3, 2003, pp. 176-185.

[8] Hodges, D. H., "Review of Composite Rotor Blade Modeling," *AIAA Journal*, Vol. 28, No. 3, 1990, pp. 561-564.

[9] Johnson, W., "Rotorcraft Dynamics Models for a Comprehensive Analysis," *Proceedings of the* 54^{th} *Annual Forum of the American Helicopter Society*, Washington, D.C., 1998.

[10] Hodges, D. H., Saberi, H., and Ormiston, R. A., "Development of Nonlinear Beam Elements for Rotorcraft Comprehensive Analyses," *Journal of the American Helicopter Society*, Vol. 52, No. 1, 2007, pp. 36-48.

[11] Theodorsen, T., "General Theory of Aerodynamic Instability and the Mechanism of Flutter," *NACA Technical Report 496*, 1935.

[12] Greenberg, M. J., "Airfoil in Sinusoidal Motion in a Pulsating Stream," *NASA Technical Report 1326*, 1947.

[13] Loewy, R. G., "A Two Dimensional Approach to the Unsteady Aerodynamics of Rotor Wings," *Journal of the Aeronautical Sciences*, Vol. 24, No. 2, 1957, pp. 81-98.

[14] Friedmann, P. P., and Venkatesan. C., "Coupled Helicopter Rotor/Body Aeromechanical Stability Comparison of Theoretical and Experimental Results," *Journal of Aircraft*, Vol. 22, No. 2, 1985, pp. 148-155.

[15] Gaonkar, G. H., McNulty, M. J., and Nagabhushanam, J., "An Experimental and Analytical Investigation of Isolated Rotor Flap-Lag Stability in Forward Flight," *Journal of the American Helicopter Society*, Vol. 35, No. 2, 1990, pp. 25-34.

[16] Cernicchiaro, A., Coppotelli, G., Mastroddi, F., and Gennaretti, M. "Analysis of Helicopter Cabin Vibrations Due to Rotor Asymmetry and Gust Encounter," AIAA Paper No. 2003-1518, *Proceedings of the* 44^{th} *AIAA/ASME/ASCE/AHS/ACS Structures, Structural Dynamics and Materials Conference*, Norfolk, Virginia, April 2003.

[17] Lee, H. G., Viswamurthy, S. R., and Shin, S. J., "Coupling of a Geometrically Exact Rotor Blade Analysis with Unsteady Aerodynamics and Dynamic Inflow," *American Helicopter Society Specialist's Conference on Aeromechanics*, San Francisco, CA, Jan., 2008.

[18] Pitt, D. M., and Peters, D. A., "Rotor Dynamic Inflow Derivatives and Time Constants from Various Inflow Models," *Proceedings of the* 9^{th} *European Rotorcraft Forum*, Stresa, Italy, Sept. 1983.

[19] Peters, D. A., Boyd, D. D., and He, C. J., "Finite-State Induced-Flow Model for Rotors in Hover and Forward Flight," *Journal of the American Helicopter Society*, Vol. 34, No. 4, 1989, pp. 5-17.

[20] Leishman, J. G., and Crouse, G. L., "State-Space Model for Unsteady Airfoil Behavior and Dynamic Stall," AIAA Paper 89-1319, *Proceedings of the* 30^{th} *AIAA/ASME/ASCE/AHS/ASC Structures, Structural Dynamics and Malerials Conference*, Mobile Alabama, April 3-5, 1989.

[21] Meyer, M., and Matthies, H. G., "State-space Representation of Instationary Two-dimensional Airfoil Aerodynamics," *Journal of Wind Engineering and industrial Aerodynamics*, Vol. 92, 2004, pp. 263-274.

[22] Leishman, J. G., and Nguyen, K. Q., "State-space Representation of Unsteady Airfoil Behavior," *AIAA Journal*, Vol. 28, No. 5, 1990, pp. 836-844.

[23] Petot, D., "Differential Equation Modeling of Dynamic Stall," *La Reserche Aérospatiale*, No. 1989-5, 1989.

[24] Petot, D. "Errata to Differential Equation Modeling of Dynamic Stall," *Private Communication*, 2005.

[25] Truong, V. K., "Oscillatory Behavior of Helicopter Rotor Airloads in the Blade Stall Regime," *Journal of Aircraft*, Vol. 32, No. 5, 1995, pp. 1148-1149.

[26] Srinivasan, G. R., Baeder, J. D., Obayashi, S., and McCroskey, W. J., "Flowfield of a Lifting Rotor in Hover: A Navier - Stokes Simulation," *AIAA Journal*, Vol. 30, No. 10, 1992, pp. 2371-2378.

[27] Strawn, R. C., Caradonna, F. X., and Duque, E. P. N., "30 Years of Rotorcraft Computational Fluid Dynamics Research and Development," *Journal of the American Helicopter Society*, Vol. 51, No. 1, 2006, pp. 5-21.

[28] He, Cheng Jian., "Development and Application of a Generalized Dynamic Wake Theory for Lifting Rotors," *Ph.D. Thesis*, Georgia Institute of Technology, July 1989.

[29] Laxman, V., and Venkatesan, C., "Chaotic Response of an Airfoil due to Aeroelastic Coupling and Dynamic Stall," *AIAA Journal*, Vol. 45, No. 1, 2007, pp. 271-280.

[30] Laxman, V., and Venkatesan, C., "Influence of Dynamic Stall and Dynamic Wake Effects on Helicopter Trim and Rotor Loads," *American Helicopter Society Specialist's Conference on Aeromechanics*, San Francisco, CA, Jan., 2008.

[31] Venkatesan, C., *Lecture Notes on Helicopter Technology*, Department of Aerospace Engineering, IIT Kanpur.

[32] Padfield, G. D., *Helicopter Flight Dynamics*, Blackwell Science Ltd, 1996.